AMERICAN UNIVERSITY OF BEIRUT

EQUILIBRIUM DYNAMICS OF A POLYMER CHAIN END-ATTACHED TO AN ADSORBING SURFACE

by
WASSIM ALI SLEIMAN

A thesis
submitted in partial fulfillment of the requirements
for the degree of Master of Science
to the Department of Physics
of the Faculty of Arts and Sciences
at the American University of Beirut

Beirut, Lebanon
February 2021

AMERICAN UNIVERSITY OF BEIRUT

EQUILIBRIUM DYNAMICS OF A POLYMER CHAIN END-ATTACHED TO AN ADSORBING SURFACE
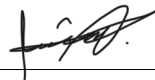
by
WASSIM ALI SLEIMAN

Approved by:

LKlushin

_____

Dr. Leonid Klushin, Professor   Advisor

Physics

_____

Dr. Jihad Touma, Professor   Member of Committee

Physics

_____

Dr. Michel Kazan, Professor   Member of Committee

Physics

Date of thesis defense: February 22, 2021

AMERICAN UNIVERSITY OF BEIRUT

THESIS, DISSERTATION, PROJECT RELEASE FORM

Student Name: __SLEIMAN_____WASSIM_____ALI___
           Last   First   Middle

☑ Master's Thesis   ◯ Master's Project   ◯ Doctoral Dissertation

☑   I authorize the American University of Beirut to: (a) reproduce hard or electronic copies of my thesis, dissertation, or project; (b) include such copies in the archives and digital repositories of the University; and (c) make freely available such copies to third parties for research or educational purposes.

☐   I authorize the American University of Beirut, to: (a) reproduce hard or electronic copies of it; (b) include such copies in the archives and digital repositories of the University; and (c) make freely available such copies to third parties for research or educational purposes after: **One ___ year from the date of submission of my thesis, dissertation or project.**
Two ___ years from the date of submission of my thesis , dissertation or project.
Three ___ years from the date of submission of my thesis , dissertation or project.

_____   February 27, 2021
       Signature   Date

Acknowledgements

An Abstract of the Thesis of

Wassim Ali Sleiman   for   Master of Science
Major: Physics

Title: Dynamics of the Adsorption-Desorption Transition of A Polymer Near A Plane

In this thesis we investigate the problem of a single polymer chain one-end-grafted to a surface of adjustable attraction strength. Particularly we introduce a locally defined adsorption order parameter and analyze its spatial and temporal correlations to check the consistency of the "blob" picture. We first check the accuracy of our molecular dynamics simulations by reproducing known results pertaining to mean number of adsorbed monomers $\langle M \rangle$, mean height of the chain's free end $\langle Z_{end} \rangle$, and mean parallel-to-surface component of the chain's gyration radius $\langle R_{G\parallel} \rangle$. We then characterize the scaling of the system in the adsorption regime, finding dynamic dependencies such as $\tau_{Zend} \propto \langle Z_{end} \rangle^{3.67}$, $\tau_{RG\parallel} \propto \langle Z_{end} \rangle^{-0.5}$, and $\tau_{Zend} \propto \tau_M$ to hold very well against predictions of scaling theory in conjunction with Rouse model dynamics. The relation between Z_{end} taken as a measure of the adsorption blob size, and the correlation length measured along the chain contour did not take the expected form. Finally, the ratio of the adsorption relaxation time of individual monomers to the global relaxation time, τ_{mi}/τ_M was analyzed as a function of the adsorption strength. For large enough N, it shows a sharp drop at the transition point, but both relaxation times scale with N in the same way irrespective of the adsorption regime.

Contents

List of Figures

XI

List of Tables

Chapter 1

Introduction

Recent groundbreaking technological advancements, such as atomic force microscopy (AFM) and optical tweezers, have jumpstarted the field of single-chain phase transition, a big and important branch of soft-matter physics. We have been able to perform single-chain manipulations since 1986 [7] ; quantities we are capable of measuring or estimating for a single chain include but are not limited to its elasticity [8, 9], the strength of the adhesion forces [10], and unfolding response to sticking/slipping off a surface [11].

The motivation behind this work comes from biology: studies have been conducted to measure the folding, unfolding, stretching, and adsorption of protein and DNA strands to cell membranes and other cellular structures. The dynamics of adsorbed polymers finds itself in many fields, from biophysics to material science. It is applied in the study of polymer-coated colloids, and polymer brushes.

On the experimental front, works have been done on the statics and dynamics of macromolecules in different environments. In 2000, Oesterhelt et al. conducted

unfolding experiments on bacteriorhodopsin proteins by pulling them away from a mica surface [12]. AFM was used to pull on one of their monomers while one of the ends is grafted to the surface. This showed how helical structures within the protein individually unfolded and interacted with each other. Building on these findings, Kessler et al. wrote in 2006 about the refolding of these same proteins [13]. This allowed to estimate the magnitude of the forces felt by the helical structures. In 2005, Hugel et al. qualitatively compared force-extension curves of three different polymer architectures [9], and found good agreement with ab-initio theoretical calculations, while in 2006, Kühner et al. measured the end-to-end distance and the contour length of pinned carboxy-methyl-amylose molecules using AFM [14], and were able to find its Kuhn length and scaling exponent.

The above work was largely done by biologists and biophysicists studying living organisms. These organisms are made up of substructures such as membranes, proteins, DNA strands etc... which are not yet fully understood on the physical level. They fall under the class of soft matter, which is a class distinct from other types of matter such as fluids and solids, due to its interesting and complex properties [15]. Other examples of soft matter are gels, polymer melts, and liquid crystals. But polymers actually are fundamental components of a large number of biological systems, particularly because proteins and DNA are classified as such. It is therefore necessary, if we want to study living organisms, to understand polymer physics. Biologists and biophysicists measure all kinds of interesting polymer-related observables that help understand and better model biological systems. But to fundamentally understand the behavior of such complex systems, we need to fully understand the simple picture of a single polymer

at an interface [16, 17, 18].

In the present work, we look at a specific aspect of a polymer's adsorption-desorption transition. Phase transitions are a class of phenomena known to occur in bulk matter under certain conditions, but not exclusively. Soft matter can also undergo phase transitions, and more specifically, polymers have shown peculiar characteristics when viewed in the scope of critical phenomena. Many biological processes have been observed to be based on phase transitions of macromolecules, which only goes to strengthen the argument for studying polymer phase transitions. Here we study a polymer grafted by one end to a hard surface of varying interaction parameter, and free at the opposite end.

The general setting is as follows: a single-stranded long chain of N bonded monomers exists in the vicinity of a hard flat surface, the latter being located at the plane $z = 0$. One end of the chain is strongly attached (grafted) to the surface (typically at $x = y = z = 0$), while the other end is left unconstrained and free. What distinguishes the present setting from the regular free-chain one are two things: the presence of the surface itself, which makes the system anisotropic, and the monomer-surface interaction, which in terms of energy is given an effective value -ϵ (it is negative because the interaction is attractive, so the tendency for the polymer is to get adsorbed since the system tends to lower its energy). The order parameter—the parameter we choose to study to classify the system in terms of its changes, typically ranging between 0 and 1—turns out to be the fraction of adsorbed monomers, which is simply the fraction of monomers that is interacting with the surface. If M is the number of adsorbed monomers and N is the total number of monomers making up the polymer, then the order parameter would be $m = M/N$, and it has been fundamental in the study of this system.

A phase transition can be seen when looking at the chosen order parameter as a function of the interaction energy ϵ. Figure 1.1 shows this: the order parameter is nearly null for all ϵ less than some value, and grows towards 1 for ϵ above this value. We call where the two ranges meet the region of the critical point. The critical point of adsorption is the point where the system's order parameter switches from 0 to 1. In phase transition theory, this switch can happen abruptly or smoothly. In other words, the order parameter can either experience a discontinuity (a jump) at the critical value ϵ^*, or it can be smooth, while one of its derivatives experiences said discontinuity. When the former takes place, we say that the transition is discontinuous or of the first order, and when the latter happens we describe the transition as a continuous one, of the n-th order, where the discontinuity happens in the n-th derivative. Other properties of the system have also been investigated, such as spatial dimensions normal and parallel to the surface, and relaxation times of the adsorption number and the height of the free end. More on this will be expanded in chapter 2.

It is also worth noting that the system has been also studied with two sets of control variables and order parameters [1]. While the system undergoes a phase transition when looking at m as a function of ϵ alone, Zhang et al. showed that the system exhibits richer behavior when a force is also applied to the free end of the chain and the stretching degree is taken as the force's conjugate order parameter. Said stretching can be written as the height of the free-end monomer from the surface, divided by the number of monomers: $\xi = \frac{z_{end}}{N}$. The resultant phase diagram is shown in figure 1.2. The applied force is taken to be vertical only, which distinguishes between positive (stretching) and negative (pressing) values of F and makes the critical value $F^* = 0$. The interplay between the two
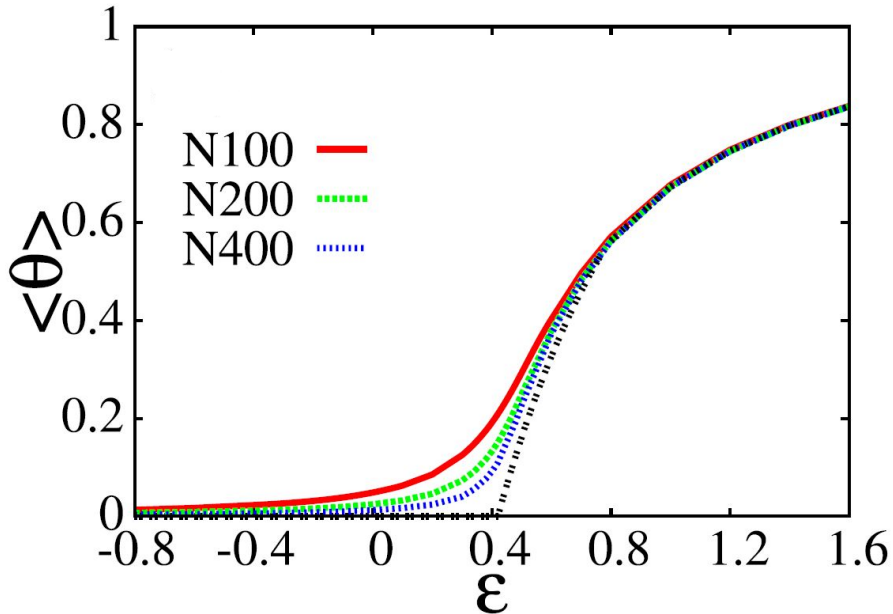
Figure 1.1: Taken from Zhang et al. [1]. Mean adsorption fraction $\langle \theta \rangle$ as a function of adsorption strength ϵ for chains of 100 (red), 200 (green dashed), and 400 (blue dashed) monomers. Black dotted line represents the transition in the thermodynamic limit; it has a corner close to $\epsilon = 0.4$, indicating the phase transition. Important to note that the simulations that gave this plot also employed a pressing force on the free end monomer, meaning that our simulations will not be identical, and we should not expect the change in m to start at the same value shown here.

control variables is mostly interesting in the positive-positive quadrant: for both $f > 0$ and $\epsilon > 0$, the polymer is being mechanically pulled off of the surface by the upward pulling force. The line $f = \epsilon$ divides the quadrant and represents the first-order transition between adsorbed polymer and stretched polymer configurations. The two negative semi-axes ($f = [0; -\infty]$ and $\epsilon = [0; -\infty]$) are two continuous transitions, and where the three lines meet, we get a critical point ($f = 0; \epsilon = 0$).

Theoretically, polymer adsorption was first tackled in 1953 [19]. In a letter to the Journal of Chemical Physics, Frisch, Simha, and Eirich derived the partition
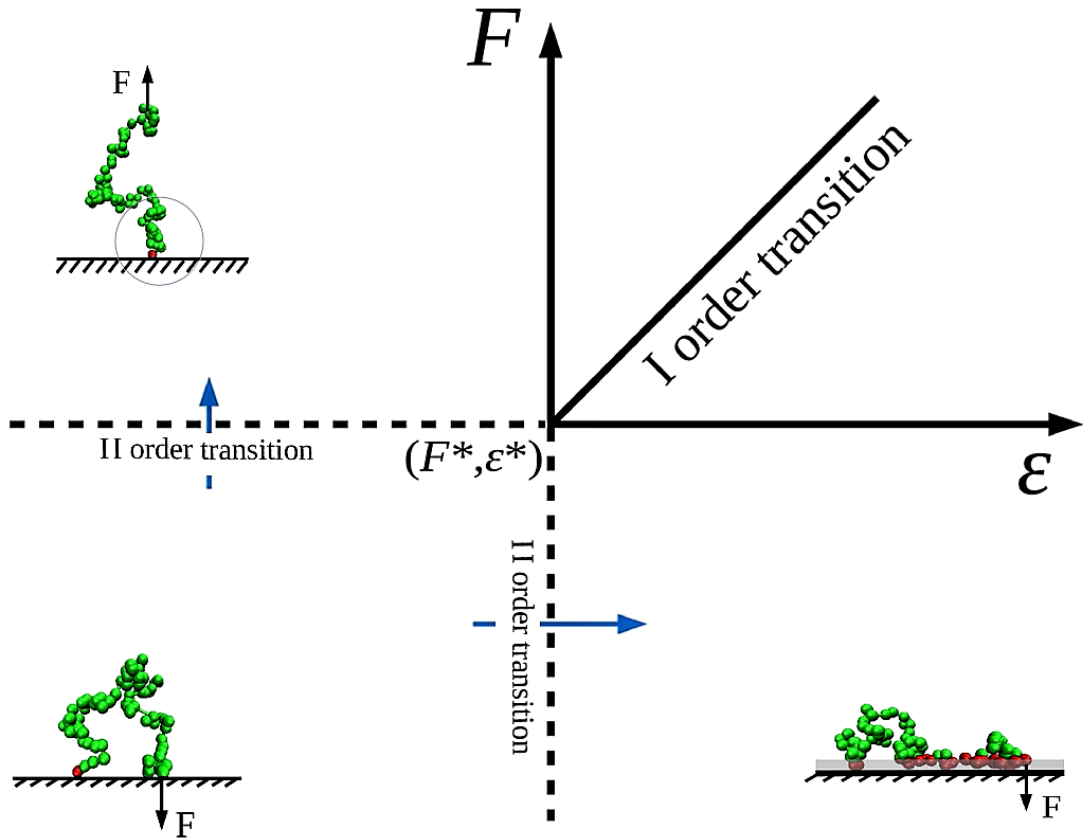
Figure 1.2: Taken from Zhang et al. [1]. Schematic sketch of Polymer adsorption-desorption and loop-stretch phase diagram.

function of a dilute solution of polymers near a weakly adsorbing surface. In the thermodynamic limit ($N \longrightarrow \infty$), they predicted that all events of adsorption would be of single monomers. Later in 1965, a study by Robert Rubin looked at the adsorption of an isolated chain to a surface using a random-walk lattice model [20]. They determined the average number of adsorbed monomers as a function of the adsorption energy and the length of the chain $M(\epsilon, N)$, the mean distance of the free end of the chain from the surface $z(\epsilon, N)$ along with its probability distribution as a function of height above the surface, and a lattice-dependent critical adsorption energy ϵ_c. In 1977, Lépine and Caillé theoretically compared the two cases of single-end-grafted and both-ends-grafted polymers at a hard

surface for three surface types (reflective, attractive, and repulsive) [21]. The criteria compared were thickness of adsorption layer, the mean number of adsorbed monomers, and the mean distance from the surface. Results were in good agreement with lattice model studies for the single-end-grafted polymer, and only differed quantitatively for the both-ends-grafted polymer. Skvortsov, Gorbunov, and Klushin introduced the idea of stretching the polymer by pulling its free end upwards, in 1993 [2]. They were able to write a closed analytical form of the partition function, and draw the phase diagram which turned out to be symmetric under exchange of the pulling force and adsorbing strength parameters. Then in 2004, Descas, Sommer, and Blumen presented extensive Monte Carlo simulations which focused on the mean number of adsorptions, the chain's extension, and the density profile for all monomers [22]. They also were able to estimate the value of the scaling exponent, but found that its value is significantly sensitive to changes in the value of the critical adsorption strength. In addition, it was found that the dynamic scaling at ϵ^* matched quantitatively that of free chains. De Gennes proposed in his work [25] that a coarse-graining approach to the chain in the adsorption regime leads to a renormalized 2D chain of "adsorption blobs" at the interface, allowing for further connections to be built between the chain's different spatial dimensions and relaxation times. An in-depth analysis of the phase transitions followed in 2012 by Skvortsov et al. [23]. Two ensembles were probed: the force ensemble, in which the control variable is the constant force applied to the free end of the polymer, and the z-ensemble, in which the height z of the free end of the polymer is the variable. It turned out that basic thermodynamic parameters such as the energy of adsorption behave differently in each of the ensembles. The continuity of the transition also differed. This work also drew similarities and differences between said transition and the vapor-liquid one, and

7

introduced the concept of local order parameter profiles. Lastly, in 2017, Zhang et al. showed in a paper that for a tethered chain that is being pulled away from the surface, characteristic relaxation time grew as a power law as ϵ_c was approached [1]. Also, they noted that the mixture of continuous transition features with the discontinuous transition features could be a phenomenon characteristic of force-driven transitions of macromolecules.

The focus of this thesis is on the nature of the adsorption order parameter. While all the previous work was based on studying the system in terms of global variables and a global adsorption order parameter (defined as the adsorption fraction of the whole chain), we attempt to characterize the system in local terms as well. More specifically, we define a local order parameter as the contact probability for a given monomer, and study the correlation length along the chain contour and the local equilibrium relaxation times of adsorption as a function of the control parameter, ϵ, and the chain length, N. We compare the local and the global descriptions and connect them to the commonly accepted blob picture [25] taking the height of the free end $Z_{end}(\epsilon)$ as a measure of the blob size. In section 2.4, we develop theoretical predictions for the correlation length and the adsorption relaxation times in terms of the blob size, Z_{end}, which also gives them as implicit functions of the control parameter ϵ. The blob theory predictions are then compared to the simulation results. In addition we attempt to quantify the adsorption event in terms of the local energy of interaction with the surface, and compare the results to those based on a more traditional definition in terms of an ad hoc cut-off distance.

Chapter 2

Theoretical Background

2.1 Chain and Solvent

In this chapter, we put forward the theoretical considerations underlying our work. It is more than fair to note that this chapter uses and references mostly the works and results authored by M. Rubinstein and R. Colby [24] for the sections on the different types of chains and scaling laws (see also the book by P. G. de Gennes [25]), and C. W. Gardiner [26] for the section on stochastic dynamics.

We use the model of a real chain in a good solvent. To understand the characteristics of this model, one must know the difference between ideal and real chains, and between different types of solvents.

Ideal chains' monomers interact with each other as long as they are close to each other along the chain. Meaning, if the monomers are successively numbered from 1 to N, then monomer i feels the interaction from only the monomers j close to i; the interaction between monomers vanishes for $|i - j| >> 1$. The unphysical consequence of this limited interaction is that monomers that are far

away along the chain but close together in space will not interact. They may even overlap without repelling each other. This is where a real chain comes in handy: this model simply allows all monomers to interact with each other, regardless of along-the-chain distance. This obviously comes at a great computational cost. The first step is to give all monomers their own volume, also called excluded volume because this volume is occupied by the one monomer and does not allow other monomers to take part of it: overlap is forbidden. This is called hardcore repulsion. The second step is to assign an additional monomer-monomer interaction. Monomers could attract each other, and they could also repel each other. The interplay of the hardcore repulsion with the added attraction/repulsion decides whether the polymer would tend to collapse into a globule, or swell into coil configurations that are more swollen the stronger the repulsion. specifics of this interaction will be discussed along with the ones of the solvent next.

The role the solvent plays is essential, simply because adsorption is mediated by it. In the simplest case, we have a homopolymer (a polymer made from only one type of monomer) in solution. We distinguish two types of particles: monomers and solvent particle. This entails three types of interactions: monomer-monomer, solvent-solvent, and monomer-solvent interactions, each characterized by a mean interaction energy. The solvent can be characterized when these three energies are put together in the flory interaction parameter

$$\chi = \frac{z}{2} \frac{(2u_{MS} - u_{MM} - u_{SS})}{kT}. \tag{2.1}$$

Using this parameter, we can get the monomers' effective excluded volume according to $v_{eff} = (1 - 2\chi)v_0$, which then simplifies characterizing the solvent. It

is worth mentioning that as χ is inversely proportional to the temperature T, one can speak of that or the other interchangeably, keeping in mind the correct limits. Given all possible combinations of interaction energies between the species, we can sum up the types of solvents as the following:

- **for $\chi \to 0$ or high temperatures,** the value of the excluded volume approaches v_0. At this limit the excluded volume is a very slowly varying function of temperature, hence the effective interaction here can be modeled as pure hard-core repulsion. **We are in an Athermal solvent**.

- **for $0 < \chi < 1/2$ and intermediate temperatures,** we have $0 < v < v_0$. In this regime the monomers feel slight attraction, which reduces their excluded volume to values below the hard-core volume. The effective interaction here can be modeled as purely repulsive as well, but with "smaller monomers" than that of an athermal solvent. **We are in a Good solvent**.

- **for $\chi = 1/2$** the excluded volume is exactly equal to zero, which is equivalent to the case of an ideal chain, and the polymer will obey ideal chain statistics, having a mean end-to-end distance of []. In this case, effectively, there is no interaction between monomers far away from each other along the chain. **We are in θ(Theta)-solvent**.

- **for $\chi > 1/2$ or low temperatures,** we get a negative excluded volume, and the polymer collapses into a globule. Here the interaction needs to have both attraction for large and intermediate distances, and repulsion for short distances. **We are in a Poor solvent.**

Now that it is clear what a real chain in a good solvent is, we justify our choice by recognizing that on one hand, a real chain model is more pertinent to

real-life applications, while on the other hand good solvent regime is the most interesting and useful of the regimes.

2.2 Chain Near a Surface and Adsorption Events

2.2.1 Chain Near a Surface

Polymer and solvent have been individually looked at. We now consider the environment. Having a substrate and a polymer together in space does not guarantee their interaction, and it would be a waste of time and opportunity to have the polymer drift around for long times without coming into contact with the surface. For this reason the polymer is grafted by one of its free ends to the surface. The chain therefore starts immediately at the interface.

For a real chain in a good solvent, the mean end-to-end distance is

$$R_F = (va^2 N^3)^{1/5}.$$

When near a purely hard surface, thermal fluctuations knock about the monomers and are bound to bring some of them to the plane of the surface (say the plane $z = 0$), where they will feel an abrupt force that pushes them away and back into the allowed half-space. This asymmetry causes a change in R_F.

We are interested in the behavior of the system as a function of the adsorption strength, so instead of a hard surface interaction which is infinite at and beyond the wall and zero before it, we give the surface an interaction parameter ϵ such that a monomer gains energy $E(z, \epsilon)$ when it is said to be "in contact" with the surface. As a consequence to this definition, an attractive surface has positive ϵ, lowers monomers' energies when they make contact, making it favorable to ad-

sorb; which is what we exactly expect from an attractive surface. The mirrored opposite can be said for a repulsive surface.

We add that when a polymer is very close to an impenetrable surface, its configuration space becomes limited and a force of entropic nature pushes the polymer away from the surface. The most likely configurations for a polymer tethered to a hard or repulsive surface are called mushroom-like, because a "stem" starts from the grafted monomer and a coil-like configuration will dominate in the remainder of the chain, far from the reach of the surface's repulsion. The probable configurations in the case of an attractive surface are different; for moderate attraction strength the number of adsorption events is substantially increased, with long segments being adsorbed to the surface. At high attraction strength the polymer is forced onto the surface, describing a 2D random walk.

2.2.2 Adsorption Events

An adsorption event can be defined in different ways. As was mentioned previously, the potential chosen for the surface to interact with the polymer is a Lenard-Jones potential, of maximum depth ϵ. The potential is zero at a distance σ from the plane. We have two options to define an adsorption event: the definition that is mainly used in the literature is any monomer (with the exception of the grafted one) that is between heights $z = 0$ and some multiple of σ (say, $z = 2.5\sigma$) counts as adsorbed, and the number of adsorbed monomers is just the simple counting of monomers within that height range. The second option is to calculate the total energy of interaction between all monomers and the surface and divide it by an effective potential strength, giving the average number of adsorbed monomers $< M >$. We shall mainly focus on the simple counting as it

is the established method in the literature, but we will also use energy counting for the purpose of comparing the two methods and their results.

After implementing these definitions into the program, we acquire the number of adsorbed monomers $M(t)$, from which we can get the adsorbed fraction as a function of time

$$m(t) = \frac{M(t)}{N}, \tag{2.2}$$

the second-order cumulants of adsorption (see section 2.3.1)

$$C_2 \propto \frac{\langle m^2 \rangle - \langle m \rangle^2}{\langle m \rangle^2}, \tag{2.3}$$

both with respect to the surface attraction strength ϵ. In addition, we can get from this data the auto-correlation functions of $M(t)$ against time, of individual monomers' adsorption state $m_i(t)$ against time, and the along-the-chain adsorption correlation functions $m_i(k)$, for every ϵ.

2.3   Global Quantities and Scaling

2.3.1   Scaling Theory and Contact Number

Scaling theory will present the theoretical framework with which we compare our simulation results. Finite size scaling proposes writing the partition function of a polymer undergoing the desorption-adsorption transition as

$$Q_\epsilon(\epsilon, N) = Q_\epsilon(\epsilon^*)\Psi_\epsilon[(\epsilon - \epsilon^*)N^\phi] \tag{2.4}$$

where ϕ is called the crossover exponent. In tandem with equation 2.4, the scaling approach also relies on reasoning for the limits of M. One can intuitively be convinced that for very weak surface attraction values we get

$$\langle M \rangle \sim N^0,$$

because contacts are unfavorable. For strong surface attraction values we expect nearly the whole chain to be adsorbed, so

$$\langle M \rangle \sim N^1.$$

As for the critical point, we define ϕ such that for $\epsilon = \epsilon^*$,

$$\langle M \rangle = N^\phi.$$

Plenty of work [17, 27, 22, 28] has been done to measure ϕ; for a while different values were debated, and an upper and lower bounds were proposed. The literature finally settled on the most accurate estimate of $\phi = 0.483 \pm 0.003$ [27, 28], while accepting the value $\phi = 0.5$ for chains lengths similar to the ones explored in this work [28].

In equation 2.4, Ψ_ϵ is called the crossover function, because it governs the vicinity of the critical energy in the partition function through its dependence on the factor $(\epsilon - \epsilon^*)$. This gives equation 2.4 important implications: having dependence on the interaction energy ϵ exclusively in Ψ_ϵ means that we can write

for the average contact number

$$\langle M \rangle = \frac{\partial \ln \Psi((\epsilon - \epsilon^*)N^\phi)}{\partial \epsilon} \qquad (2.5)$$

and for the fluctuations of M

$$\sigma^2(M) = \langle M^2 \rangle - \langle M \rangle^2 = \frac{\partial^2 \ln \Psi((\epsilon - \epsilon^*)N^\phi)}{\partial^2 \epsilon}. \qquad (2.6)$$

Knowing the expected asymptotic behavior of $\langle M \rangle$, we can get that of $\Psi_\epsilon(x)$, where the scaling variable is

$$x = (\epsilon - \epsilon^*)N^\phi. \qquad (2.7)$$

In fact, equation 2.5 can be written as

$$\langle M \rangle = N^\phi f_M((\epsilon - \epsilon^*)N^\phi) \qquad (2.8)$$

where

$$f_M(x) \propto \frac{\partial \ln \Psi(x)}{\partial x}$$

is the scaling function of M around criticality. This means that if we attempt to plot $\langle M \rangle / N^\phi$ against $(\epsilon - \epsilon^*)N^\phi$, lines of different N values should collapse onto one master-curve which represents the scaling function itself. The quality of this collapse is a measure of the quality of the combination $[\epsilon^*, \phi]$, because the master-curve depends on both those values. Hence we are presented with a benchmark that serves to check our critical energy and crossover exponent values pair. However, we note that we use this method as a check only, and not to determine the values of $[\epsilon^*, \phi]$. This is because determination of the values using

16

the fit quality of the mastercurve gives us the two values depending on each other; both parameters are being tuned simultaneously, and are therefore not independent. In other words, it was found [] that a small difference in ϵ^* would lead to large deviations of ϕ if this method is used to *determine* instead of *check for agreement* [22, 29].

From the above expectations of $\langle M \rangle$ we can write the asymptotes of $\ln \Psi_\epsilon$, and then get more detailed predictions for the asymptotes of 2.5 and 2.6. We summarize those asymptotes here[1]:

$$\ln \Psi_\epsilon(x) \begin{cases} \ln(-x), & \text{for } x \ll -1 \\ c_1' x + c_2' x^2, & \text{for } |x| \ll 1 \\ x^{1/\phi}, & \text{for } x \gg 1 \end{cases} \tag{2.9}$$

$$\langle M \rangle \begin{cases} \frac{1}{\epsilon^* - \epsilon}, & \text{for } x \ll -1 \\ N^\phi, & \text{for } |x| \ll 1 \\ N(\epsilon - \epsilon^*)^{\frac{1-\phi}{\phi}}, & \text{for } x \gg 1 \end{cases} \tag{2.10}$$

$$\sigma^2(M) \begin{cases} \frac{1}{(\epsilon^* - \epsilon)^2}, & \text{for } x \ll -1 \\ N^{2\phi}, & \text{for } |x| \ll 1 \\ N(\epsilon - \epsilon^*)^{\frac{1-2\phi}{\phi}}, & \text{for } x \gg 1 \end{cases} \tag{2.11}$$

Given

$$\langle M \rangle = \frac{\partial \ln \Psi_\epsilon((\epsilon - \epsilon^*)N^\phi)}{\partial \epsilon} \propto N^\phi$$

17

(equation 2.10), and

$$\sigma_M^2 = \frac{\partial^2 \ln \Psi((\epsilon - \epsilon^*)N^\phi)}{\partial^2 \epsilon} \propto N^{2\phi}$$

(equation 2.11), we take the ratio in equation 2.3, giving

$$\frac{\sigma_M^2}{\langle M \rangle^2} = \frac{\frac{\partial^2 \ln \Psi(x)}{\partial^2 x}}{\left(\frac{\partial \ln \Psi_\epsilon(x)}{\partial x}\right)^2},$$

which is itself a function of the variable $x = (\epsilon - \epsilon^*)N^\phi$. This means that exactly at the critical point, regardless of the length of the polymer, $c2$ has the same value. The fact that these cumulants have the same value exactly at $\epsilon = \epsilon^*$ for different N serves to zero in on the numerical value of the critical energy: plotting the cumulants of polymers of different degrees of polymerization against ϵ reveals a point of intersection, whose abscissa corresponds to the critical adsorption strength ϵ^*[refer to BINDER]. Once found, the value of ϵ^* will allow a more clear-cut comparison of the system's behavior on each end.

2.3.2   Scaling of Spatial Components

In the previous section we showed how $\langle M \rangle$ scales with N away from and near the critical point, as a test of our simulations. We also take interest in some spatial components of the system for the same purpose. Particularly, we take two components, one being parallel to the surface (we choose the mean gyration radius component parallel to the surface, $\langle R_{G\parallel} \rangle$) and the other perpendicular to it (we choose the mean height of the free end, $\langle Z_{end} \rangle$).

The scaling forms of these quantities can be written [30] as:

$$Z_{end} = N^{\nu_{3D}} h_\perp((\epsilon - \epsilon^*)N^\phi) \tag{2.12}$$

$$R_{G\parallel} = N^{\nu_{3D}} h_\parallel((\epsilon - \epsilon^*)N^\phi), \tag{2.13}$$

with $h_\perp$ and $h_\parallel$ being the corresponding scaling functions. For $\epsilon \ll \epsilon^*$ and $\epsilon = \epsilon^*$ the different dimensions of the chain scale with N the same way a free self-avoiding chain does [31, 30]:

$$\langle Z_{end} \rangle \sim \langle R_{G\parallel} \rangle \sim N^{\nu_{3D}},$$

with $\nu_{3D} \approx \frac{3}{5} = 0.6$ being the Flory exponent in three dimensions.

However, in the adsorption regime things do not behave the same way. For $\epsilon \gg \epsilon^*$ one can intuitively expect that

$$\langle Z_{end} \rangle \sim N^0$$

when picturing the flat configurations allowed in this regime. For a very attractive surface it was shown [24] that the polymer will be almost completely adsorbed into a layer of thickness ξ right above the surface, with a tail of height $Z_{end} \sim \xi$. As for $\langle R_{G\parallel} \rangle$, intuition also says that, since conformations in this regime are nearly two dimensional at the surface, scaling with N is that of a 2-D self-avoiding chain:

$$\langle R_{G\parallel} \rangle \sim N^{\nu_{2D}}.$$

$\nu_{2D} = 3/4$ here is the Flory exponent for a self-avoiding chain in two dimensions. In the same way we wrote the mean values of Z_{end} and $R_{G\parallel}$ using the two functions

19

in 2.13, which are proportional to the first derivative of the natural logarithm of the partition function, we can write analogously the fluctuations of the two spatial components by using the second derivatives. The limits for said fluctuations turn out to be:

$$\sigma^2(Zend) \begin{cases} N^{2\nu_{3D}}, & \text{for } x \ll -1 \\ N^{2\nu_{3D}}, & \text{for } |x| \ll 1 \\ N^0, & \text{for } x \gg 1 \end{cases} \tag{2.14}$$

$$\sigma^2(RG \parallel) \begin{cases} N^{2\nu_{3D}}, & \text{for } x \ll -1 \\ N^{2\nu_{3D}}, & \text{for } |x| \ll 1 \\ N^{2\nu_{2D}}, & \text{for } x \gg 1 \end{cases} \tag{2.15}$$

We will further expand on the dependencies of quantities of interest (and their relaxation times) in the strong attraction regime in section 2.4.

2.3.3 Dynamics, Correlations, and Scaling of Relaxation Times

To get temporal correlation, we can write the autocovariance of the number of adsorbed monomers M_t at a time t as

$$K_{MM}(\tau) = \frac{1}{T}\sum_{t=1}^{T}(M_t - \langle M \rangle)(M_{t+\tau} - \langle M \rangle) = \frac{1}{T}\sum_{t=1}^{T}M_t M_{t+\tau} - \langle M \rangle^2 \tag{2.16}$$

where τ is a time interval, T is the time of the simulation, and $\langle M \rangle$ is the average number of adsorbed monomers over time at equilibrium. Normalizing by

$$\sigma^2 = K_{MM}(\tau = 0)$$

we get the time-dependent Pearson correlation coefficient, which we will call for simplicity the Autocorrelation function:

$$\rho_{MM}(\tau) = \frac{K_{MM}(\tau)}{K_{MM}(0)} \tag{2.17}$$

As for spatial correlation, we are interested in those between different monomers as a function of the distance between them along the backbone of the polymer. We therefore compute the adsorption correlation functions along the chain, averaged over time. We define said functions as

$$\rho_s(k) = \frac{K_s(k)}{K_s(0)}, \tag{2.18}$$

where

$$K_s(k) = \frac{1}{N - k} \sum_{i=1}^{N-k} (s_i - \langle s_i \rangle)(s_{i+k} - \langle s_i \rangle), \tag{2.19}$$

s is the adsorption state of monomer of index i, k is the distance along the chain between the pairs of monomers, and $\langle s_i \rangle$ is the mean adsorption state for monomer i over all time. It is worth noting that the values s can take depend on the definition of adsorption event used.

Seeing that we are studying the system at equilibrium, we expect the process to be a wide-sense stationary one. This allows the use of a Fourier and an Inverse

Fourier transforms, giving the correlations with much less computation time. These correlation functions give us —by integration— the characteristic times for near-equilibrium fluctuations to decay and the correlation distance of adsorption along the chain.

To theorize about these times, we use the Rouse model which approximates our chain to one that is made up of (renormalized) beads attached by springs. During its relaxation time τ, a chain is expected to diffuse a distance proportional to its own size. Adding onto that the expectation of the diffusion coefficient to be inversely proportional to N, we can write [3, 25, 32, 33] that a characteristic relaxation time is

$$\tau \propto \frac{\langle \sigma^2 \rangle}{D_N} \propto N\sigma^2.$$

σ is the fluctuation of the quantity under consideration, and D_N is the diffusion coefficient of the whole chain. This model predicts therefore that the scaling of τ with N is predicted by σ of the corresponding spatial quantity, in the following way:

$$\tau_X \sim N\sigma_X^2. \tag{2.20}$$

The Rouse model is written for times of spatial diffusion. However, if we attempt to apply it to the number of contacts M, we get for the scaling of τ

$$\tau_M \sim \begin{cases} N^1, & \text{for } x \ll -1 \\ N^{1+2\phi}, & \text{for } |x| \ll 1 \end{cases} \tag{2.21}$$

$$\tau_{Zend} \sim \begin{cases} N^{1+2\nu_{3D}}, & \text{for } x \ll -1 \\ N^{1+2\nu_{3D}}, & \text{for } |x| \ll 1 \end{cases} \tag{2.22}$$

22

$$\tau_{RG\parallel} \sim \begin{cases} N^{1+2\nu_{3D}}, & \text{for } x \ll -1 \\ N^{1+2\nu_{3D}}, & \text{for } |x| \ll 1 \end{cases} \qquad (2.23)$$

Where we remind that $x = (\epsilon - \epsilon^*)N^\phi$. We tackle scaling in the adsorption regime, and summarize the expectations in the next section.

2.4 Local Considerations and the Blob Picture

We have predicted using finite-size scaling theory the scaling laws of different spatial quantities in our system, but we have skipped the strong attraction (or adsorption) regime on purpose. The reason we do that is because we believe scaling in this regime follows different expectations, for the configurations here are substantially more restricted to a layer near the surface.

For a strongly attractive surface, one can intuitively expect (and show) the free end monomer to be in the vicinity of the surface regardless of the length of the polymer; an equilibrated polymer will be predominantly adsorbed to the surface irrespective of N, especially with increasing ϵ. In the framework of scaling theory, however, things usually relate to a "blob"; renormalization of the chain units relative to the proper scale of interest is the basic idea of scaling theory, and in the adsorption regime, the relative scale becomes that of the adsorption blob. Figure 2.1 elucidates the concept. When our chain is collapsed onto the surface due to its strong attraction, we can speak of a certain blob, a grouping of our monomers that is not arbitrary, but is done in such a way that dynamics of interest become those of monomers inside one blob only, irrelevant of the rest of the chain. In other words,the chain becomes a collection of uncorrelated parts (blobs), and

we need only to consider one part to understand the properties of the entire chain. What becomes our focus then is the dynamics of these adsorption blobs, which are by definition of the size scale relevant to experience the confinement imposed by the surface. The size of a blob ξ defines the relevant size scale of the system, which by definition is equal to the layer's thickness and to the mean height of the free end. This means that by measuring $\langle Z_{end} \rangle$ we have a direct measurement of the blob size [24]. This makes things more convenient. We can now proceed to scale relaxation times in the adsorption regime.
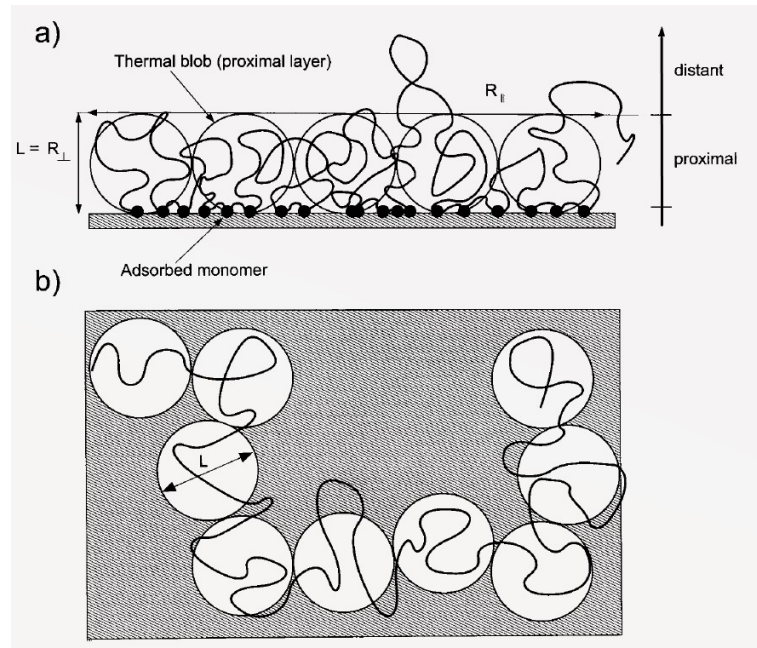
Figure 2.1: Taken from Descas, Sommer, and Blumen [3]. (a) Blob picture of chain near attractive surface, seen from the side. The chain is confined to a layer of thickness L beyond which the probability distribution of finding monomers is insignificant. (b) Top view of the blob picture. The polymer becomes a two-dimensional chain of blobs on the surface.

Since system properties depend on the blob, our relaxation time scaling will have to depend on properties of the blob instead of the whole chain. The Rouse

model gives equation 2.20, with $N \to g \sim \xi^{1/\nu_{3D}} \sim \langle Z_{end} \rangle^{1/\nu_{3D}}$ where g is the number of monomers in a blob, and $\sigma^2 \equiv \sigma^2_{Z_{end}} \sim \langle Z_{end} \rangle^2$. We thus say

$$\tau_{Zend} \sim \begin{cases} \langle Z_{end} \rangle^{2+1/\nu_{3D}}, & \text{for } x \gg +1. \end{cases} \tag{2.24}$$

In the same vein, one can argue that in the parallel-to-surface direction, we have a two-dimensional chain of blobs of characteristic blob size $\xi = \langle Z_{end} \rangle$. The number of blobs per chain is

$$n_b = N \langle Z_{end} \rangle^{-1/\nu_{3D}},$$

and the gyration radius parallel would be

$$R_{G\|} \sim \xi n_b^{\nu_{2D}} = N^{\nu_{2D}} Z_{end}^{1 - \frac{\nu_{2D}}{\nu_{3D}}}.$$

Thus we finally reach

$$\tau_{RG\|} \sim \begin{cases} N^{1+2\nu_{2D}} \langle Z_{end} \rangle^{2 - 2\frac{\nu_{2D}}{\nu_{3D}}}, & \text{for } x \gg +1. \end{cases} \tag{2.25}$$

We summarize all theoretical predictions for the scaling of all quantities of interest, their fluctuations, and their relaxation times in table 2.1.

Table 2.1: Summary of theoretically expected scaling trends for the three quantities of interest, their fluctuations, and their relaxation times.

	Pre-Adsorption Regime	Critical Point	Adsorption Regime
	$\epsilon \ll \epsilon^*$	$\epsilon = \epsilon^*$	$\epsilon \gg \epsilon^*$
$\langle M \rangle$	$\sim N^0$	$\sim N^\phi \approx N^{0.483}$	$\sim N^1$
$\langle Z_{end} \rangle$	$\sim N^{\nu_{3D}} \approx N^{0.6}$	$\sim N^{\nu_{3D}} \approx N^{0.6}$	$\sim N^0$
$\langle R_{G\parallel} \rangle$	$\sim N^{\nu_{3D}} \approx N^{0.6}$	$\sim N^{\nu_{3D}} \approx N^{0.6}$	$\sim N^{\nu_{2D}} = N^{0.75}$
σ_M	$\sim N^0$	$\sim N^\phi \approx N^{0.483}$	$\sim N^1$
$\sigma_{Z_{end}}$	$\sim N^{2\nu_{3D}} \approx N^{1.2}$	$\sim N^{2\nu_{3D}} \approx N^{1.2}$	$\sim N^0$
$\sigma_{R_{G\parallel}}$	$\sim N^{2\nu_{3D}} \approx N^{1.2}$	$\sim N^{2\nu_{3D}} \approx N^{1.2}$	$\sim N^{2\nu_{2D}} \approx N^{1.5}$
τ_{Msc}	$\sim N^1$	$\sim N^\phi \approx N^{0.483}$	$\sim N^1$
$\tau_{Z_{end}}$	$\sim N^{1+2\nu_{3D}} \approx N^{2.176}$	$\sim N^{1+2\nu_{3D}} \approx N^{2.176}$	$\sim N^0 \langle Z_{end} \rangle^{2+1/\nu_{3D}} \approx \langle Z_{end} \rangle^{3.67}$
$\tau_{R_{G\parallel}}$	$\sim N^{1+2\nu_{3D}} \approx N^{2.176}$	$\sim N^{1+2\nu_{3D}} \approx N^{2.176}$	$\sim N^{1+2\nu_{2D}} \langle Z_{end} \rangle^{2-2\frac{\nu_{2D}}{\nu_{3D}}} \approx N^{2.5} \langle Z_{end} \rangle^{-0.5}$

We can also speak of the along-the-chain correlations of adsorption. In a chain of N monomers, the average product of the local contact numbers for monomers with indices $(l, l+k)$ is $\langle m(l)m(l+k) \rangle_N$. If we define adsorption as $m_i = 0$ for $z_i > 2.5\sigma$ and $m_i = 1$ for $z_i < 2.5\sigma$, then we can write

$$\langle m(l) \rangle = P(l)$$

$$\langle m(l)m(l+k) \rangle = P(l)P(l+k|l)$$

$$\langle m(l)m(l+k) \rangle - \langle m(l) \rangle \langle m(l+k) \rangle = P(l)(P(l+k|l) - P(l+k)),$$

where $P(l)$ and $P(l+k|l)$ are respectively the *unconditional* probability of having the l-th monomer adsorbed, and the *conditional* probability to have the $l+k$-th

monomer adsorbed provided the l-th monomer is also adsorbed. This means that the dependence of the correlation function on the backbone distance k is given by the expression

$$P(l + k|l) - P(l + k). \tag{2.26}$$

For a self-avoiding chain of N monomers at the critical adsorption strength, these probabilities are defined in terms of partition functions of a chain with one (2.27) or two (2.28) end(s) attached to the surface [27],

$$\Omega_{1c}(n) \approx A_1 \omega^N N^{\gamma_{1c}-1}, \tag{2.27}$$

$$\Omega_{11c}(n) \approx A_{11} \omega^N N^{\gamma_{11c}-1}. \tag{2.28}$$

In the above partition functions, A_{1c}, A_{11c}, and ω are model dependent constants, but γ_{1c} and γ_{11c} are believed to be universal, and due to [27] we have $\gamma_{1c} \approx 1.226$ and $\gamma_{11c} \approx 0.707$. Numerically integrating for

$$\langle P(l+k|l) - P(l+k) \rangle = \frac{1}{N-k} \int_0^{N-k} \frac{\Omega_{11c}(k)\Omega_{1c}(N-l-k)}{\Omega_{1c}(N-l)} - \frac{\Omega_{11c}(l+k)\Omega_{1c}(N-l-k)}{\Omega_{1c}(N)} dl$$

gives us a theoretical prediction of how adsorption correlations go with k.

Chapter 3

Computational Approach

To carry out our study, we adopt a molecular dynamics (MD) simulations approach. In order to run the simulations two things are needed: a model that includes the necessary physics of the polymer, and an algorithm that solves the equations of motion while taking into account the mentioned physical factors of the chosen model.

3.1 Chain Model

A computational model for a polymer needs to account for various physical aspects, from the scales involved to the types of interactions. In this section we briefly introduce each aspect, and in section 3.2 we set our choices, describing the model fully.

3.1.1 Coarse Graining

The level at which the polymer behaves properly, also known as the level of coarse graining, depends on the scale at which the property of interest manifests. For

example, if we care to study the inter-nucleotide interactions in a DNA strand, our model will definitely need to include said nucleotides into the structure of the polymer. On the other hand, if we care to study the relaxation of the DNA as a chain, whose length happens to be on a much larger scale than that of the nucleotides, then we can model it as a simple semi-flexible polymer. If one uses the latter model to study inter-monomer interactions, one would get unphysical results that are far from the reality of actual DNA. For reviews on the different types of coarse graining for DNA and proteins see [34] and [35] respectively.

3.1.2   The Solvent

In most real cases, polymers are studied in solutions where they are dissolved in solvents. The type of the solvent-polymer interaction affects the equilibrium size of the polymer: a good solvent makes the polymer swell, while a poor solvent leads to the collapse of the polymer. The different types of solvents are summarized in section 2.1. Computationally, the solvent can be accounted for either explicitly or implicitly. In explicit solvent models, aside from the polymer itself, there are solvent particles that interact with each other and the monomers; the quality of the solvent is specified by the affinity between the different particle types, also as described in section 2.1. The second way is that of implicit solvent, where the solvent is simply accounted for through the type of non-bonded interactions. In the good solvent regime the interaction is purely repulsive, while it has an attractive part in the poor solvent regime.

3.1.3 The Langevin Thermostat

Collisions between the monomers and the solvent particles result in Brownian diffusion and friction. The fluctuation-dissipation theorem states that

$$\mathcal{D} = \frac{k_B T}{\zeta}$$

where $\mathcal{D}$ is the diffusion coefficient and ζ is the drag coefficient. This is known as the Einstein-Smoluchowski relation, and it can be included in the equations of motion by accounting for a drag force $F_d = -\zeta \dot{x}$ and a random force $F_r = \sqrt{2\zeta k_B T} R(t)$ where $R(t)$ is a stationary Gaussian process satisfying

$$\langle R(t) \rangle = 0$$

$$\langle R(t) R(t') \rangle = \delta(t - t')$$

.

3.1.4 Interactions

In most models, interactions between particles in a coarse grained polymer are divided into types that are defined based on the number of bodies interacting. First and foremost, two-body interactions are divided into two types:

- bonded interactions, which arise between nearest neighbors, and obey an interaction potential that keeps the monomers bound to each other;

- non-bonded interactions, which arise between polymers that are far away from each other along the chain, and reflect the quality of the solvent in implicit solvent models.
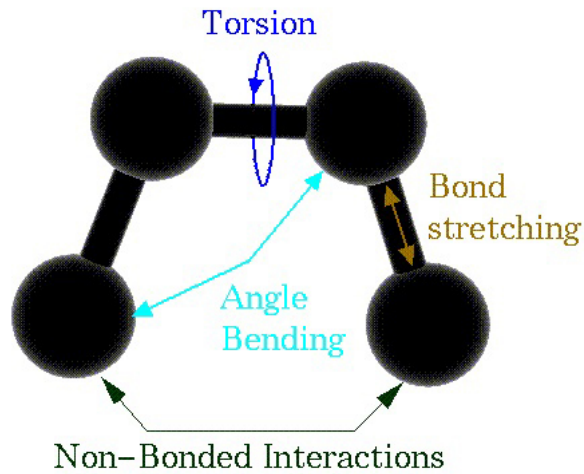
Figure 3.1: Different Types of Interactions: the brown "bond stretching" is a two-body interaction; the cyan "angle bending" is a three-body interaction; the blue "torsion" is a four-body interaction.

Some models take into account higher-order interactions, such as three-body interactions that are related to the bending of the polymer chain, and four-body interactions which are specified by the relative angles of the first and last particles in a sequence of four consecutive monomers along the chain (cf. Figure 3.1). Here we omit these higher-order interactions, and consider only two-body ones.

3.1.5 Boundaries

The polymer is restricted to a certain space bounded by rigid walls. The geometry and the interaction potential of the polymer with the wall(s) need to be specified to complete the model.

3.2 Our Model

The following sets the scene of our computational model. Coarse-graining-wise, we used a bead-spring model for the polymer. The polymer is modeled as a chain
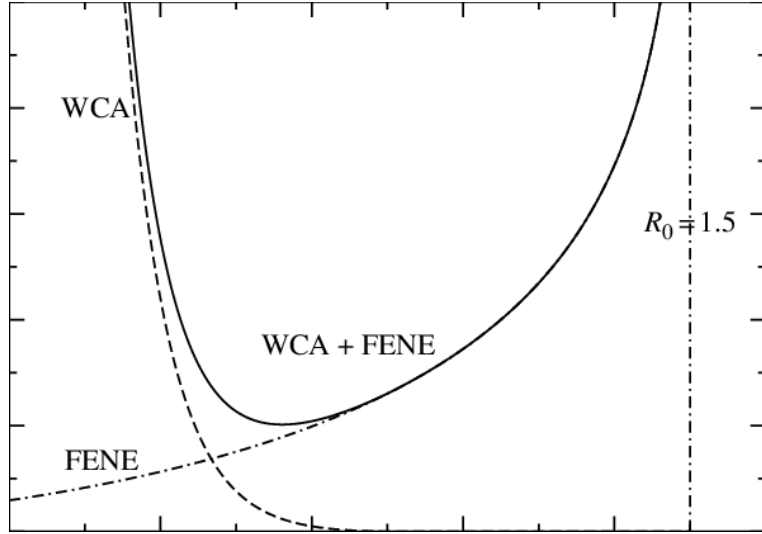
Figure 3.2: The potentials used: for non-bonded interactions (between non-successive monomers) we use the WCA (dashed line) which is the repulsive part of Lennard-Jones potential but shifted upwards; for bonded interactions (between successive monomers of the chain) we use WCA+FENE (full line) which is the overlap of the WCA and the FENE potentials, grows to infinity as it approaches the asymptote R_0 [4].

of beads connected by nonlinear springs. The solvent we used is implicit, in the good solvent regime. As for interactions, the polymer is fully flexible such that we ignore three-body and four-body interactions (see section 3.1.4); only two-body interactions were considered. The types of interactions are the following:

- Non-bonded interactions: To run the simulations in the good solvent regime we chose the repulsive part of the Lennard-Jones (LJ) potential, also known as the Weeks-Chandler-Andersen (WCA) potential (Figure 3.2):

$$U(r_{ij}) = U_{WCA}(r_{ij}) = \begin{cases} 4\epsilon\left[\left(\frac{\sigma}{r_{ij}}\right)^{12} - \left(\frac{\sigma}{r_{ij}}\right)^{6}\right] + \epsilon & \text{for } r_{ij} < r_{WCA} = 2^{1/6}\sigma \\ 0 & \text{for } r_{ij} > r_{WCA} \end{cases}$$

(3.1)
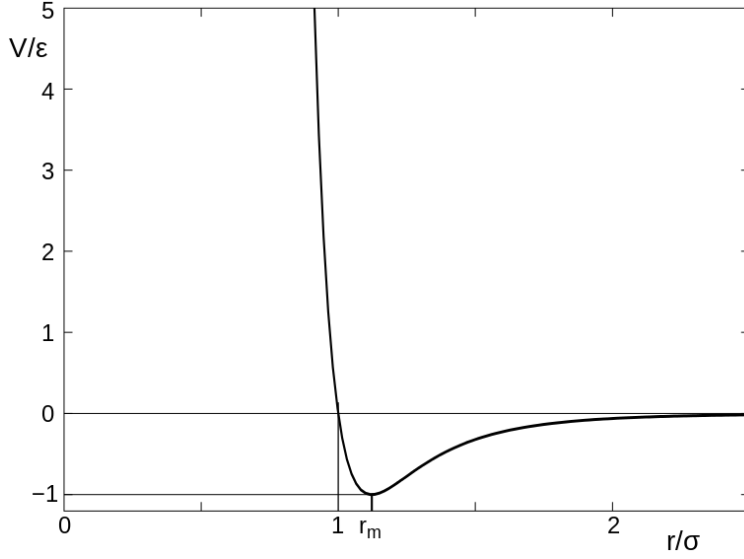
Figure 3.3: The Lennard-Jones potential used for the monomer-surface interaction. The potential is 0 at a distance σ from the $z = 0$ surface, and has a value $-\epsilon$ at its minimum, which is at $z = 2^{1/6}\sigma$ [5].

• Bonded interactions: for successive monomer-monomer interactions we use a combination of the Finitely Extensible Nonlinear Elastic (FENE) potential and the WCA potential (Figure 3.2):

$$U(r_{ij}) = U_{WCA}(r_{ij}) + U_{FENE}(r_{ij})$$

where

$$U_{FENE}(r_{ij}) = \begin{cases} -\frac{1}{2}kR_0^2 ln\left[1 - \left(\frac{r_{ij}}{R_0}\right)^2\right] & \text{for } r_{ij} \leq R_0 \\ \\ \infty & \text{for } r_{ij} > R_0 \end{cases} \quad (3.2)$$

• Surface interactions: we use the well known Lennard-Jones (LJ) potential, with a finite range of 2.5σ (Figure 3.3):

$$U_{wall}(r_{ij}) = U_{LJ}(r_{ij}) = 4\epsilon_{wall}\left[\left(\frac{\sigma_{wall}}{r_{ij}}\right)^{12} - \left(\frac{\sigma_{wall}}{r_{ij}}\right)^6\right] \quad (3.3)$$

33

For our calculations we chose $\sigma = 1$, $\epsilon = k_B T = 1$, $k = 30 k_B T / \sigma^2 = 30$, $R_0 = 1.5\sigma = 1.5$, and for the wall we chose $\sigma_{wall} = 1.0$, and the mass of a monomer is taken to be $m = 1$. To make the analogy with biological systems, taking the monomer size to be on the order of the persistence length of a typical protein, our length unit is on the order of $10\mathring{A}$. On average one amino acid has a length of $3.5\mathring{A}$, so our simulation monomer encapsulates about 3 amino acids, making the mass of a monomer around 5×10^{-25} Kg. Taking $T = 300K$, the time unit in our simulation is equivalent to about $36ps$.

3.3   The Algorithm

Next, we turn to the algorithm. A very important thing to consider while setting up molecular dynamics simulations is the choice of algorithm type to integrate the equations of motion. The most important factors to consider while making this decision are (time) efficiency and precision. For this reason, we choose the Verlet algorithm. In the following sections, we will reference Drs Frenkel and Smit's "Understanding molecular simulation: from algorithms to applications" [6]. In this book, they claim that the Verlet algorithm is both the simplest and the best one to use, for reasons we put forward in the following section.

3.3.1   The Verlet Algorithm

The aim of the algorithm is to solve the differential equations:

$$\dot{x} = v(t)$$

$$\ddot{x} = \frac{f(x, v, t)}{2m}$$

This is done by updating the current positions $x(t)$ to their new values $x(t + \Delta t)$.

The first step is to do a Taylor expansion on both the new $(x(t + \Delta t))$ and the old $(x(t - \Delta t))$ positions. We get:

$$x(t + \Delta t) = x(t) + \dot{x}(t)\Delta t + \ddot{x}(t)\Delta t^2 + \dddot{x}\Delta t^3 + \mathcal{O}(\Delta t^4)$$

$$x(t - \Delta t) = x(t) - \dot{x}(t)\Delta t + \ddot{x}(t)\Delta t^2 - \dddot{x}\Delta t^3 + \mathcal{O}(\Delta t^4)$$

Adding the two above equations, we get:

$$x(t + \Delta t) \approx 2x(t) - x(t - \Delta t) + \frac{f(t)}{m}\Delta t^2 + \mathcal{O}(\Delta t^4)$$

We can see that, given an initial position at time $t - \Delta t$ and a subsequent position at time t, and if the forces depend only on the relative positions of the particles and walls, all subsequent positions can be effectively calculated, without having to calculate velocities. Calculating velocities is important in our simulations however because of the presence of viscosity. Several methods can be derived from the Verlet method to compute velocities. Most of the computational time is spent calculating forces, which makes the choice of method for the calculation

of velocities irrelevant for speed; however, the methods differ in accuracy. We use the Velocity Verlet method outlined below:

1. Take initial positions $x_i(t)$ and velocities $v_i(t)$

2. Compute forces $f_i(t) = -\frac{dU(x_i)}{dx_i} + F_d(v_i) + F_r$ where $U(x_i)$ is the particle potential, F_d and F_r are defined in section 3.1.3

3. Update velocities by half a step using $v_i(t + \frac{1}{2}\Delta t) = v_i(t) + \frac{f_i(t)}{m}\frac{\Delta t}{2}$

4. Update positions by a full time step using $x_i(t + \Delta t) = x_i(t) + v_i(t + \frac{1}{2}\Delta t)$

5. Compute new forces $f_i(t + \Delta t)$

6. Update velocities to full time step $v_i(t + \Delta t) = v_i(t + \frac{1}{2}\Delta t) + \frac{f_i(t+\Delta t)}{m}\frac{\Delta t}{2}$

7. Repeat steps 3-5 until satisfied

3.3.2 The Verlet List

In most MD simulations, the only type of interaction that is accounted for is pairwise interaction. This means that for each iteration we need to calculate the forces for $N(N-1)/2$ pair interactions. In our simulations interactions are truncated, saving some time on force calculations. We however still need to calculate the distances between $N(N-1)/2$ pairs to check which particles interact with each other, so that the simulation time scales like N^2. A way to reduce the dependence of the computational time on the number of particles is to use a Verlet List [36]. The list of every monomer i consists of all particles within a cutoff distance r_v slightly larger than the cutoff radius for the forces r_{WCA} from particle i. During each iteration, only the distances of particles in the list will be calculated, which is a calculation of order N, and the particle i will interact with particles within the
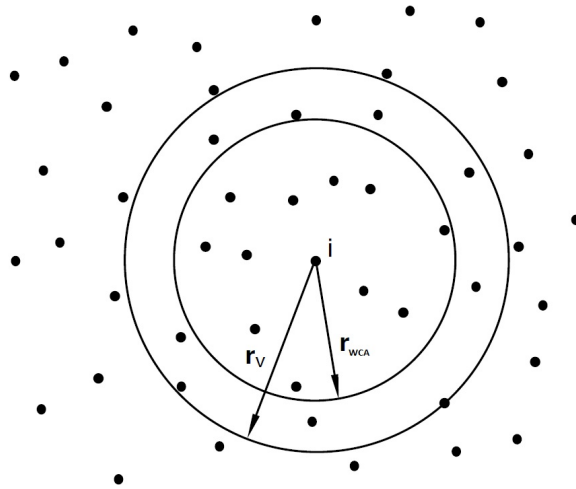
Figure 3.4: The space of the Verlet list. Particles within r_v are included in the list for particle i, while particles within r_{WCA} interact with i. Once a particle is displaced enough to leave or enter the WCA sphere, the Velrelt list is updated [6].

interaction range r_{WCA}. From time to time the list will need to be updated; the update, an operation of order N^2, will be performed whenever the displacement of any particle in the simulation exceeds $r_v - r_{WCA}$. The use of a Verlet list in the algorithm reduces the dependence of the computational time from N^2 to about $N^{3/2}$ [6].

Chapter 4

Simulation Results

We now turn to look at the results of our simulations, comparing them to the expected results based on the scaling framework. We remind the reader of a few key conventions: the number of monomers making contact with the surface M will be measured in two ways. The first by simply counting the number of monomers of heights in the range $0 \leq Z \leq 2.5\sigma$, dubbed M_{sc} for *simple counting*, and the second by calculating the total energy due to monomer-interface interactions and dividing that by the characteristic depth of the potential, ϵ, dubbed M_{ec} for *energy counting*. We discuss the latter in the last section of this chapter. Energy values are in units of $k_B T$, lengths are in units of the monomer bond equilibrium length σ, and time scales are in natural (simulation) time units. Uncertainties and bounds of confidence reported correspond to intervals of 95% confidence.

4.1 Second-Order Cumulants

Firstly, we characterize our system by locating the critical energy of adsorption. As explained in section 2.3.1, the cumulant intersection method is one of the most accurate methods to find the critical point. We plot the second-order cumulants as a function of energy for chains of lengths $N = 50, 100, 150, 200$, and 250 in figure 4.1.

The intersection seems to be in the general region $1.00 \leq \epsilon \leq 1.20$. Zooming in,
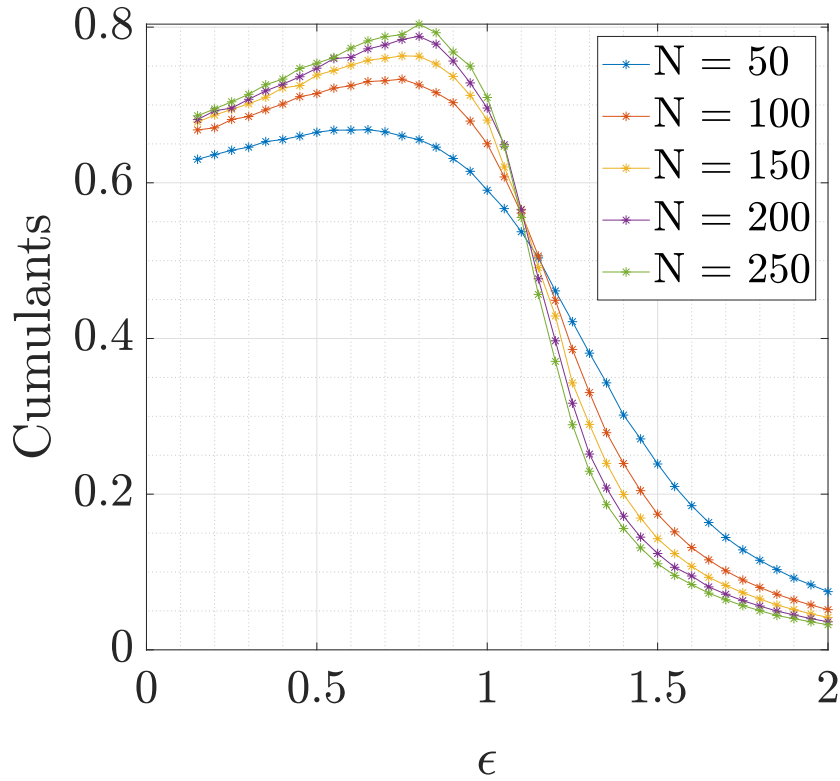
Figure 4.1: Second-order cumulants of adsorption number.

we notice multiple intersections (Figure 4.2). Calculating the arithmetic mean, we find $\epsilon^* = 1.11 \pm 0.03$.
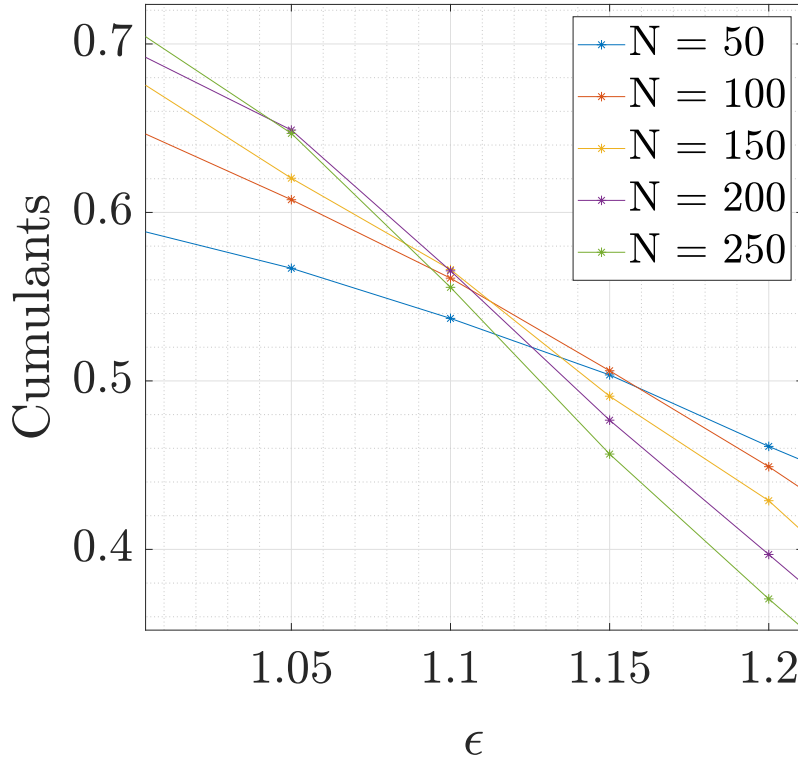
Figure 4.2: Close-up of the intersection region of the cumulants.

4.2 Statics of Quantities of Interest

We now turn our attention to the static quantities of the system: namely the mean number of adsorbed monomers $\langle M \rangle$ (4.3), the mean height of the free end $\langle Z_{end} \rangle$ (4.4), and the mean value of the component of the gyration radius that is parallel to the surface, $\langle R_{G\|} \rangle$ (4.5), along with their fluctuations (4.7 to 4.9), all as functions of the adsorption energy ϵ. As stated previously, the surface introduces an anisotropy to the problem. For this reason we look at dimensions parallel and perpendicular to the surface separately.

A superficial look tells us that the number of contacts exhibits the proper lim-

its in the weak and strong adsorption regimes; $\langle M \rangle \approx 0$ for $\epsilon = 0.15 \ll \epsilon^*$ since we expect very few contacts at these weak energies, and $\langle M \rangle \approx N$ for $\epsilon = 2.00 \gg \epsilon^*$ since we expect the entire chain to be collapsed into a two dimensional layer near the surface in this strong adsorption regime. Length components parallel and normal to the surface behave differently as was expected. In the weak attraction limit, general dimensions of the chain (both parallel and normal to the surface) obey 3-D Self-Avoiding Walk (SAW) scaling laws, governed by the Flory exponent in three dimensions $\nu_{3D} \approx 3/5 = 0.6$. In the strong adsorption regime the two dimensions separate in behavior however. While it is expected for the height of the free end to collapse to a nearly 2-D layer in the immediate vicinity of the surface, parallel dimensions increase in size because the increasing adsorption strength flattens the polymer against the surface, forcing it into a 2-D conformation that is governed by the 2-D Flory exponent $\nu_{2D} = 3/4 = 0.75$. We can see the manifestation of this basic line of reasoning in figures 4.4 and 4.5. Increasing ϵ in the former decreases the average height Z_{end}, while it increases $\langle R_{G\parallel} \rangle$ in the latter.
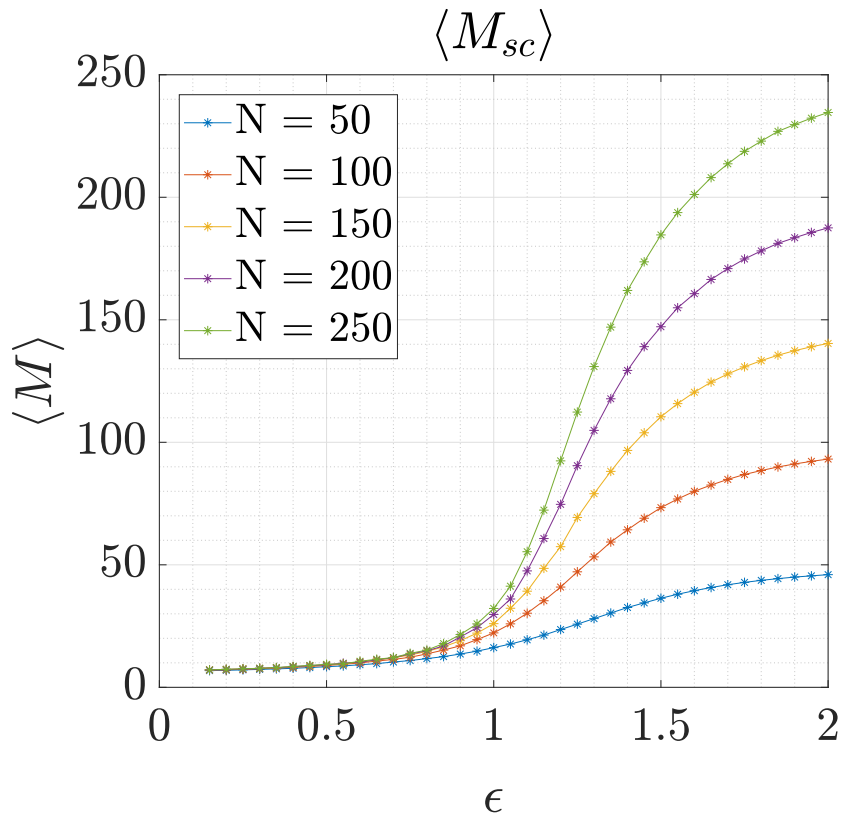
Figure 4.3: Mean number of contacts $\langle M \rangle$ as a function of adsorption strength ϵ.
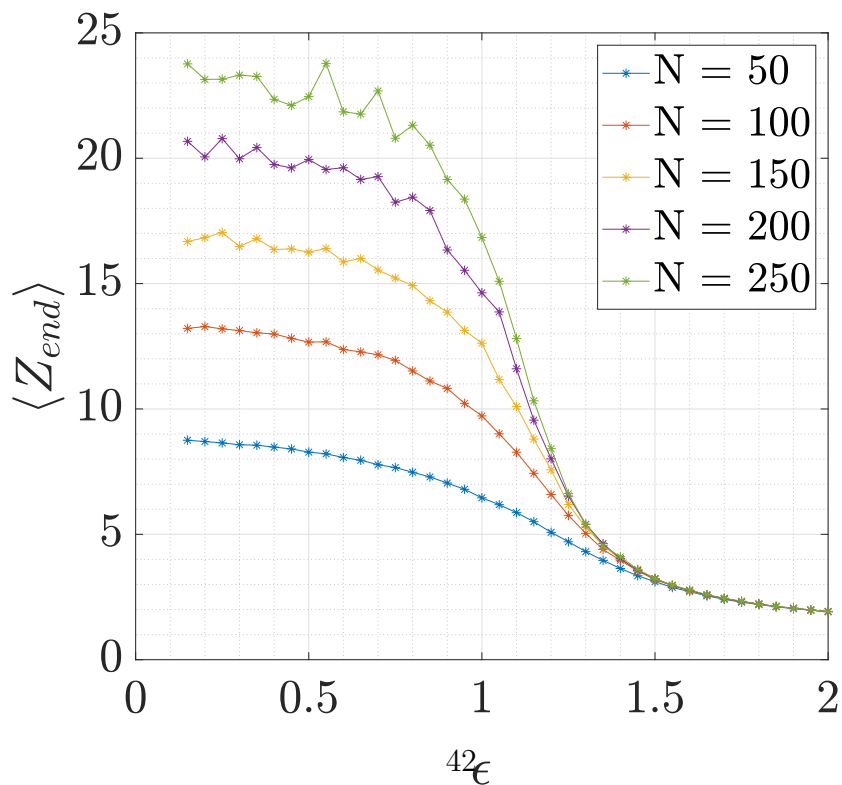
Figure 4.4: Mean height of the free end of the chain $\langle Z_{end} \rangle$ as a function of adsorption strength ϵ.
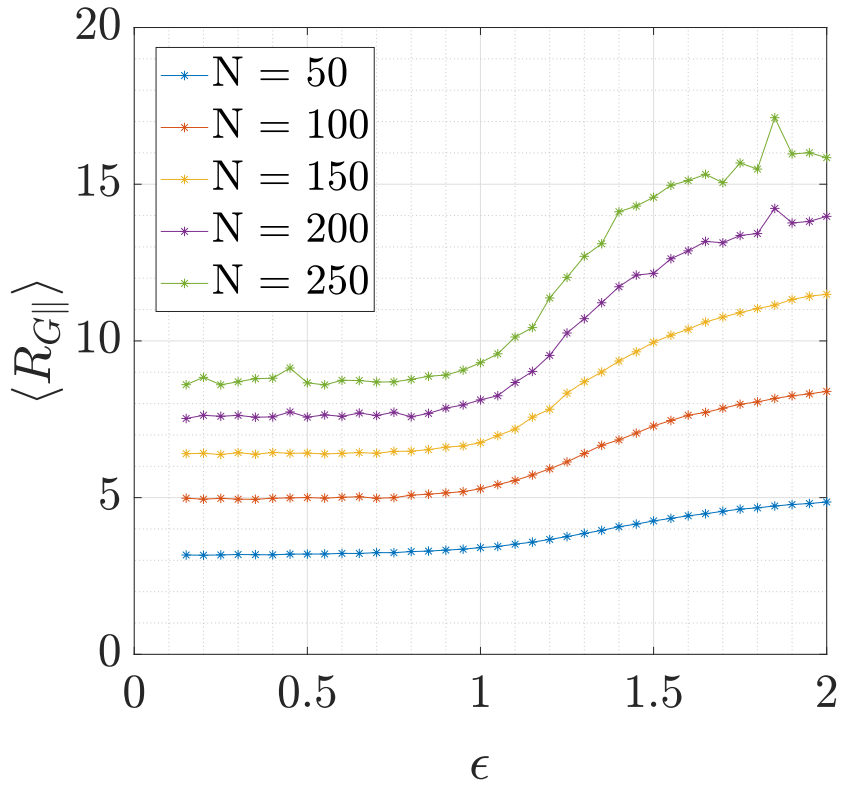
Figure 4.5: Mean value of the lateral $(X - Y)$ component of the chain's gyration radius $\langle R_{G\parallel} \rangle$ as a function of adsorption strength ϵ.

To find the dependence over N of the three quantities, we can take crossections at specific values of ϵ of the corresponding quantity, and plot their logarithms versus $\log(N)$, as we do for $\langle M \rangle$ in figure 4.6. We can then fit each set to a line to get the power of N as the slope. Tables 4.1 and 4.2 summarize the scaling exponents of the three quantities with respect to N, in all three regions. We take multiple values near the expected critical point in table 4.2 to double-check our estimate of the critical energy.
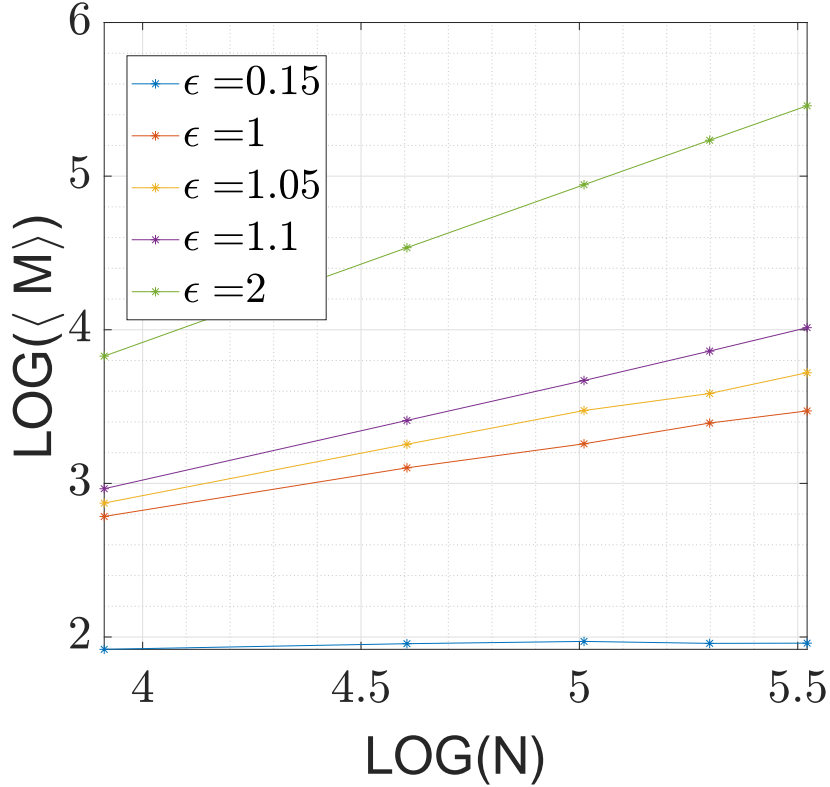
Figure 4.6: Natural logarithm plot of $\langle M \rangle$ against N for repulsion ($\epsilon = 0.15$), attraction ($\epsilon = 2.00$), and in the critical region (for three candidate energies $\epsilon = 1.00, 1.05, 1.10$).

Table 4.1: Scaling exponents for the N-dependence of quantities of interest $\langle M \rangle$, $\langle Z_{end} \rangle$, and $\langle R_{G\parallel} \rangle$ below and above the transition point, along with the theoretical predictions. $N = 50, 100, 150, 200, 250$.

	Desorption Regime		Adsorption Regime	
	$\epsilon = 0.15$	Theoretical Prediction	$\epsilon = 2.00$	Theoretical Prediction
$\langle M \rangle_{sc}$	0.020 ± 0.015	0	1.0130 ± 0.0020	1
$\langle Z_{end} \rangle$	0.620 ± 0.020	0.6	0.0030 ± 0.0020	0
$\langle R_{G\parallel} \rangle$	0.620 ± 0.015	0.6	0.74 ± 0.04	0.75

Table 4.2: Scaling exponents for the N-dependence of quantities of interest $\langle M \rangle$, $\langle Z_{end} \rangle$, and $\langle R_{G\parallel} \rangle$, in the vicinity of the transition point, along with the theoretical predictions. $N = 50, 100, 150, 200, 250$.

	Critical Point Region			
	$\epsilon = 1.00$	$\epsilon = 1.05$	$\epsilon = 1.10$	Theoretical Prediction
$\langle M \rangle_{sc}$	0.428 ± 0.010	0.52 ± 0.02	0.65 ± 0.06	$\phi \approx 0.483$
$\langle Z_{end} \rangle$	0.596 ± 0.012	0.56 ± 0.03	0.490 ± 0.007	0.6
$\langle R_{G\parallel} \rangle$	0.624 ± 0.004	0.630 ± 0.010	0.655 ± 0.006	0.6

In both the weak and strong adsorption regimes our intervals of uncertainty nicely include all predicted values, except for $\langle M_{sc} \rangle$. In the critical region we compare our values of the first row of 4.2 to the most recently accepted value of $\phi = 0.483 \pm 0.003$. Our findings suggest that $\epsilon = 1.05$ is the safest estimate of the critical energy, while the value ($\epsilon^* = 1.11$) corresponding to the cumulant intersection method overestimates ϕ noticeably.

Next we discuss the corresponding fluctuations, defined for each quantity as $\sigma_X = \sqrt{\langle X^2 \rangle - \langle X \rangle^2}$. Figures 4.7, 4.8, and 4.9 show the fluctuations, and tables 4.3 and 4.4 show the scaling with N along with the values we predict. These scaling powers of N are retrieved in the same way throughout the entire thesis, by plotting the logarithm of the quantity of interest against the logarithm of the variable whose scaling we are investigating, linearly fitting said plot, and taking the slope.
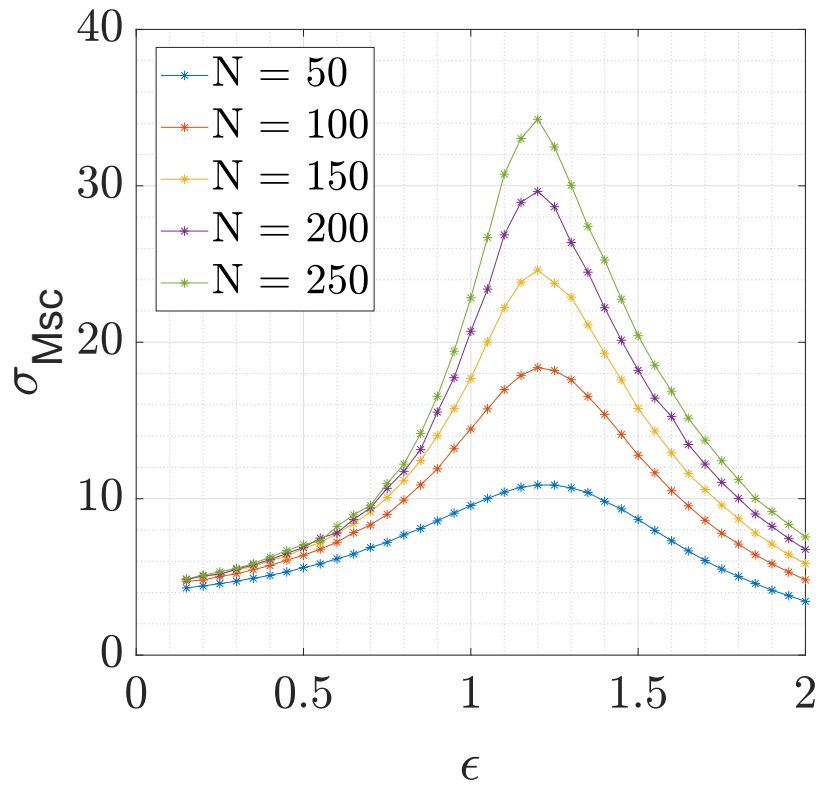
Figure 4.7: Fluctuation σ_M of the number of contacts M as a function of adsorption strength ϵ.
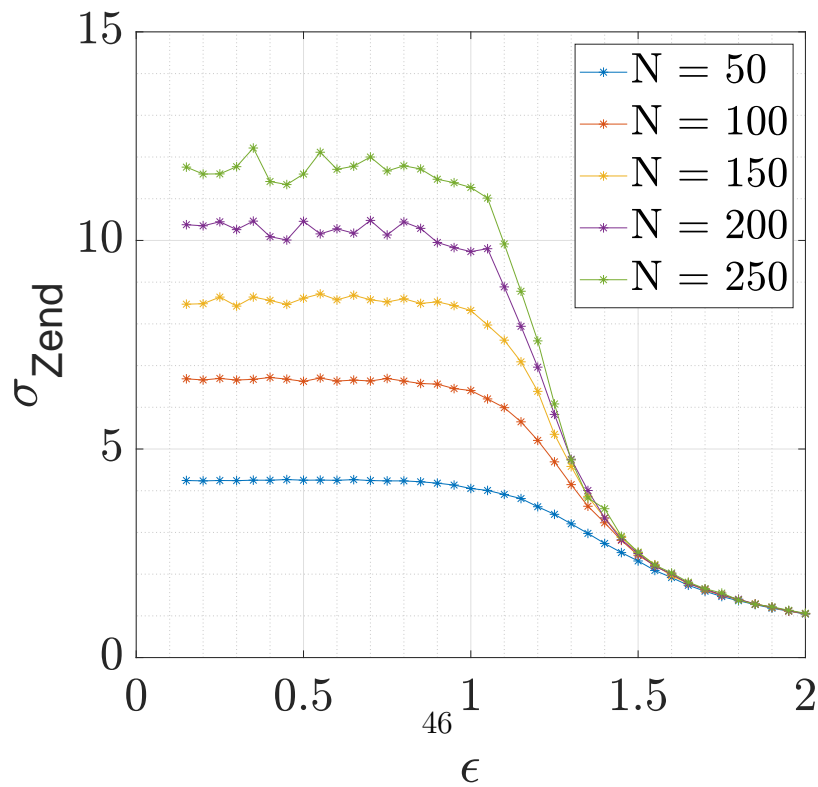
Figure 4.8: Fluctuation σ_{Zend} of the height of the free end Z_{end} as a function of adsorption strength ϵ.
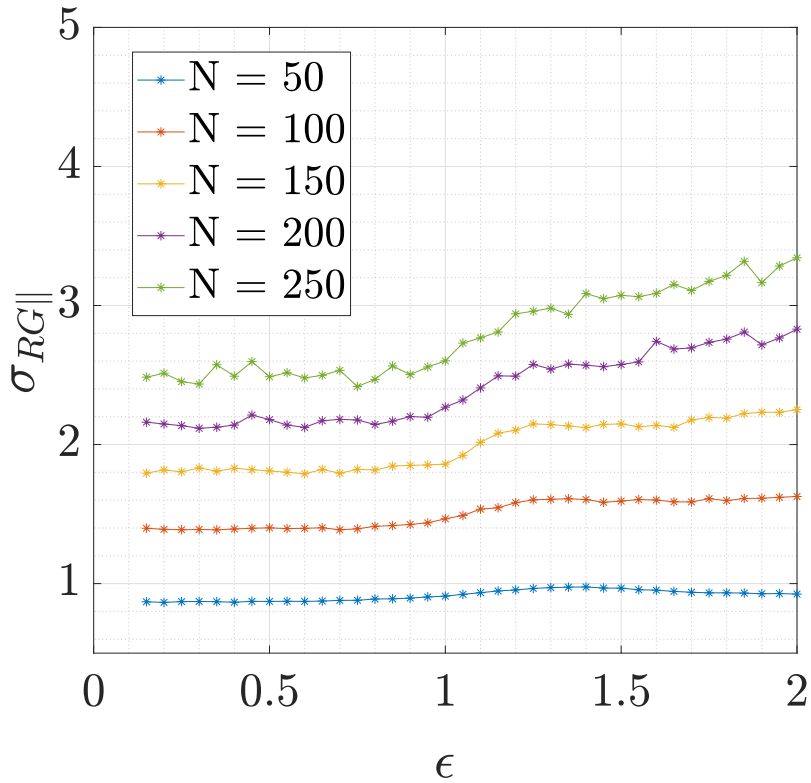
Figure 4.9: Fluctuation $\sigma_{RG\parallel}$ of the lateral component of the gyration radius $R_{G\parallel}$ as a function of adsorption strength ϵ.

Table 4.3: Scaling exponents for the N-dependence of the fluctuations σ_M, $\sigma_{Z_{end}}$, and $\sigma_{R_{G\parallel}}$, below and above the transition point, along with the theoretical predictions. $N = 50, 100, 150, 200, 250$.

	Desorption Regime		Adsorption Regime	
	$\epsilon = 0.15$	Theoretical Prediction	$\epsilon = 2.00$	Theoretical Prediction
σ_{Msc}	0.08 ± 0.06	0	0.490 ± 0.007	0.5
$\sigma_{Z_{end}}$	0.63 ± 0.03	0.6	0.010 ± 0.007	0
$\sigma_{R_{G\parallel}}$	0.65 ± 0.03	0.6	0.801 ± 0.012	0.75

In the weak and strong adsorption regimes (table 4.3) our simulations reproduce the expected scaling neatly for the fluctuations of all three considered

Table 4.4: Scaling exponents for the N-dependence of the fluctuations σ_M, $\sigma_{Z_{end}}$, and $\sigma_{R_{G\parallel}}$, in the vicinity of the transition point, along with the theoretical predictions. $N = 50, 100, 150, 200, 250$.

	Critical Point Region			
	$\epsilon = 1.00$	$\epsilon = 1.05$	$\epsilon = 1.10$	Theoretical Prediction
σ_{Msc}	0.54 ± 0.04	0.61 ± 0.04	0.67 ± 0.06	$\phi \approx 0.483$
$\sigma_{Z_{end}}$	0.63 ± 0.03	0.63 ± 0.03	0.58 ± 0.04	0.6
$\sigma_{R_{G\parallel}}$	0.65 ± 0.03	0.670 ± 0.025	0.68 ± 0.04	0.6

quantities. The same goes for the spatial components' fluctuations, when in the critical vicinity (table 4.4). As for the fluctuations of the number of contacts at the three candidate energies, they predict less accurately a cross-over exponent in a range of $0.45 \leq \phi \leq 0.73$ (including uncertainties). Only at $\epsilon = 1.00$ do we get $\phi = 0.54 \pm 0.09$, which includes the literature value of 0.483 in its uncertainty interval.

As a last check of both values of critical energy and cross-over exponent, we plot the scaled number of contacts $\log(\langle M \rangle N^{-\phi})$ against the scaled unitless energy $\log \frac{(\epsilon - \epsilon^*)}{(\epsilon^*)} N^\phi$ (see section 2.3.1). We can compare the two sets of values, $[\epsilon, \phi] = [1.11, 0.64]$ gotten from the cumulant method and subsequent fit, and $[\epsilon, \phi] = [1.05, 0.52]$, in terms of their collapse onto the same master-curve for all different values of N. We present said master-curves in figures 4.10 and 4.11.
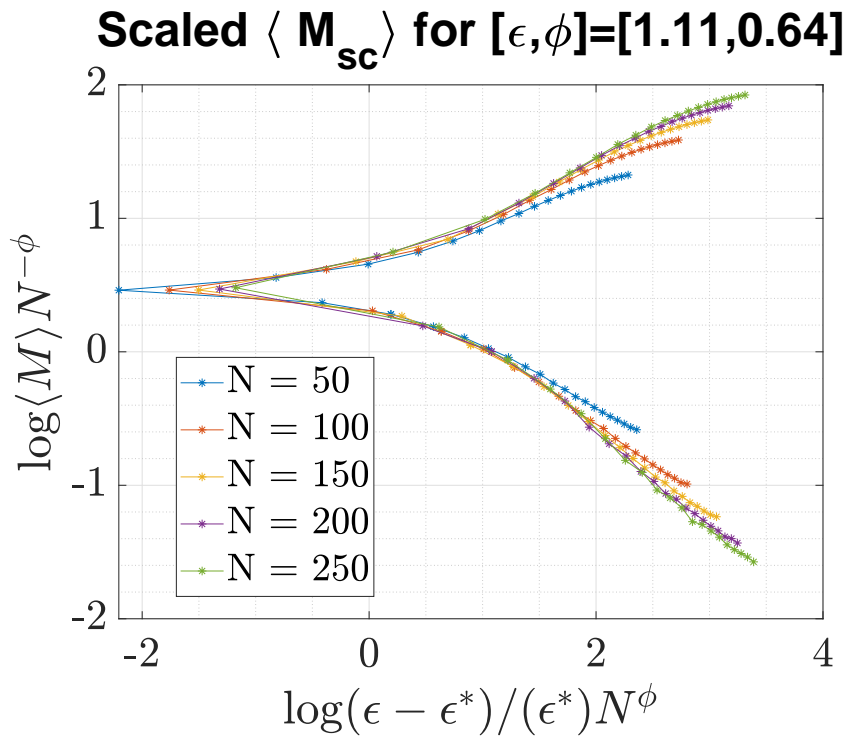
Figure 4.10: log-log plot of the rescaled number of contacts $\langle M \rangle N^{-\phi}$ as a function of the normalized scaling variable $\frac{(\epsilon - \epsilon^*)}{(\epsilon^*)} N^{\phi}$, for the pair of values $[\epsilon^*, \phi]=[1.11, 0.64]$.
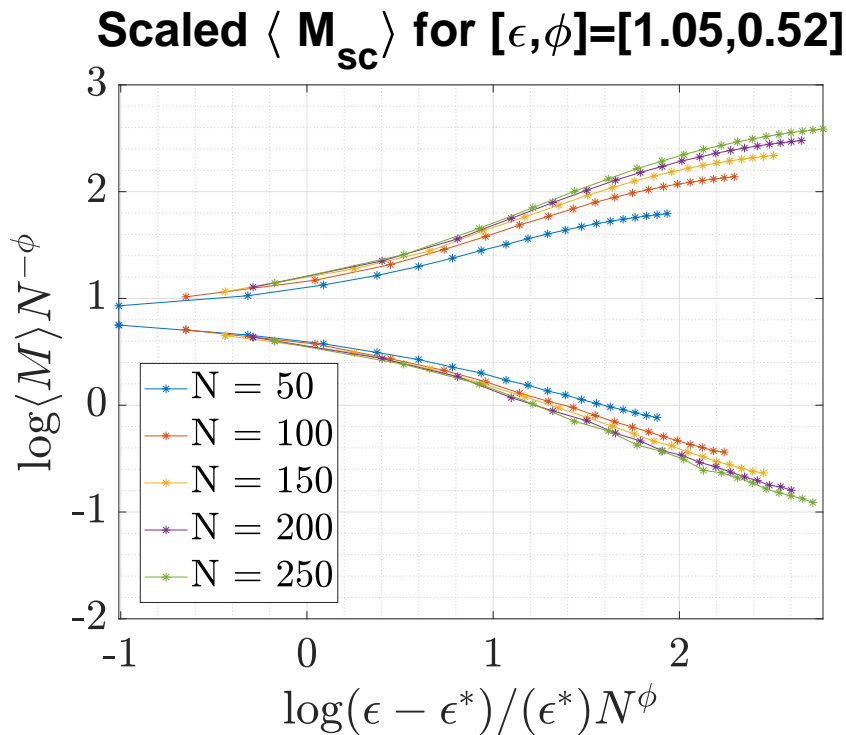

Figure 4.11: Same as figure 4.10, but for the pair of values $[\epsilon^*, \phi]=[1.05, 0.52]$.

The collapse onto a master-curve is significantly better for $[\epsilon, \phi] = [1.11, 0.64]$, the values which correspond to the cumulants intersection method.

With the presented values, we can say with a good degree of confidence that our simulations reproduce the proper static scaling behaviors. We can move now to consider the dynamical properties of the system.

4.3   Dynamical Considerations: Relaxation Times

The quantities we have been interested in so far are the number of contacts M, the height of the free end Z_{end}, and the parallel component of the gyration radius $R_{G\parallel}$. We wish to characterize the system's dynamics by considering how things change as a function of time. This study however remains one of equilibrium, so we can rightfully expect that the static means of the quantities and their corresponding fluctuations will not change with time. For this reason we focus on their correlations (and auto-correlations) as functions of time, discussed in more detail in 2.3.3.

We show the time auto-correlation functions of M, Z_{end}, and $R_{G\parallel}$ in figures 4.12 to 4.14, for $N = 250$ uniquely for conciseness. Each figure shows the auto-correlations at all the energies we have been considering, color-coded as follows: blue lines correspond to the energies in the weak adsorption regime, red lines to the strong adsorption regime, and green lines to the energies close to the critical value of ϵ.
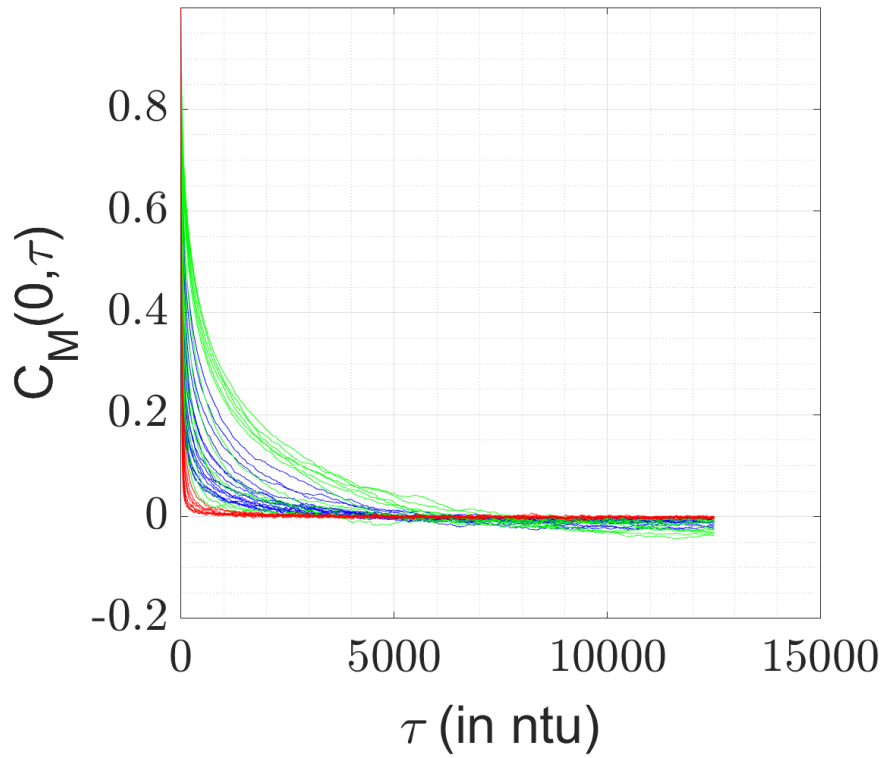
Figure 4.12: Time Autocorrelation functions of number of contacts for a chain of 250 monomers, shown for all values of ϵ. Blue lines are for the desorption regime, red ones are for the adsorption regime, and green ones are for energies in the critical vicinity.
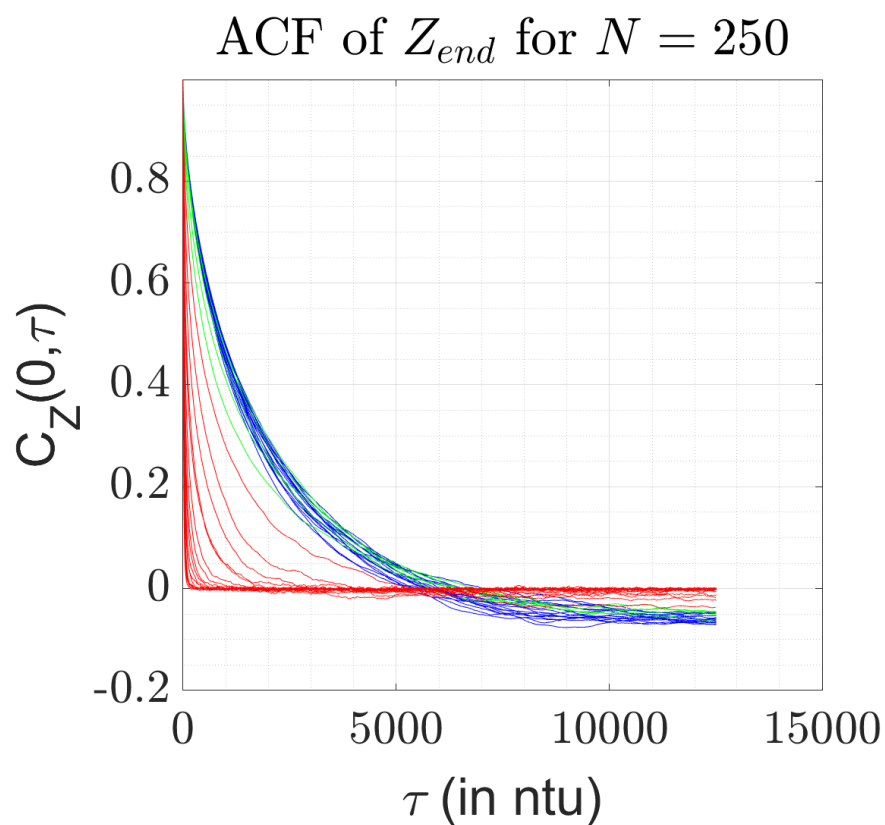
Figure 4.13: Time Autocorrelation functions of Z_{end} for a chain of 250 monomers, shown for all values of ϵ. Same color scheme as figure 4.12.

52
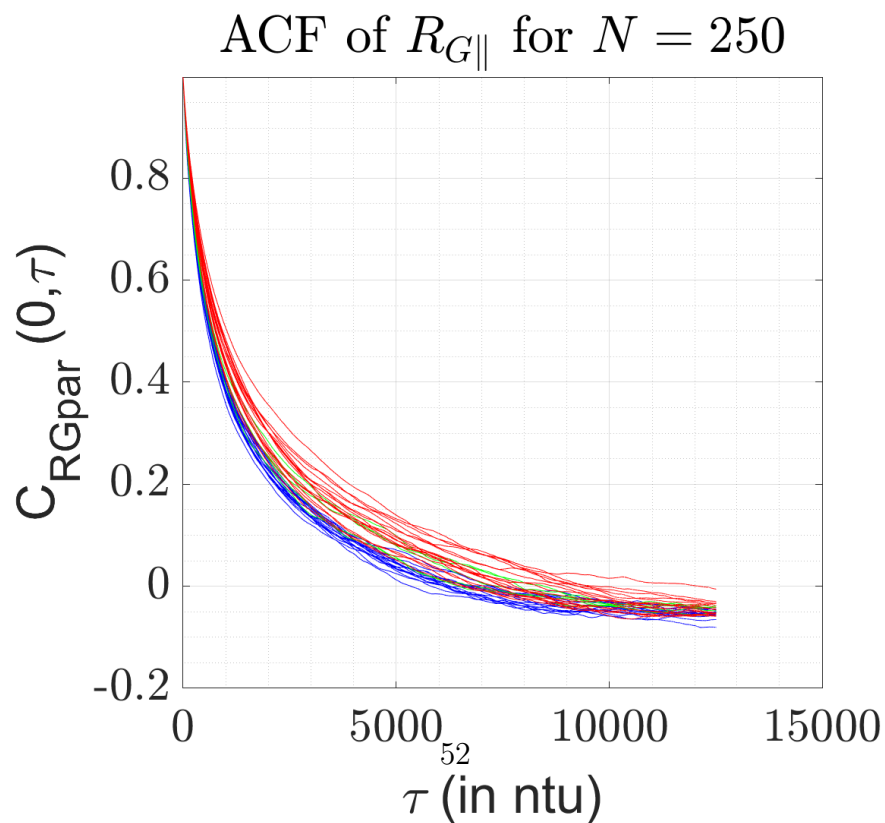
Figure 4.14: Time Autocorrelation functions of $R_{G\parallel}$ for a chain of 250 monomers, shown for all values of ϵ. Same color scheme as figure 4.12.

These correlation functions are later integrated to get the slowest time of relaxation. In other words, we integrate the correlation functions to get an estimate of the time it takes the value of the variable to fluctuate and forget itself.

We present the relaxation time profiles in figures 4.15 to 4.17. A similar basic analysis to the one employed for the static averages can be used here. We promptly summarize how these times scale with N, and state the expected scaling from the theoretical framework: see tables 4.5 and 4.6.

Figure 4.15: Relaxation times of M as function of ϵ for different values of N.

Figure 4.16: Relaxation times of Z_{end} as function of ϵ for different values of N.

Figure 4.17: Relaxation times of $R_{G\parallel}$ as function of ϵ for different values of N.

Table 4.5: Scaling exponents for the N-dependence of the relaxation times τ_M, $\tau_{Z_{end}}$, and $\tau_{R_{G\parallel}}$, below and above the transition point, along with the theoretical predictions. $N = 50, 100, 150, 200, 250$.

	Desorption Regime		Adsorption Regime	
	$\epsilon = 0.15$	Theoretical Prediction	$\epsilon = 2.00$	Theoretical Prediction
τ_{Msc}	1.10 ± 0.15	1	0.37 ± 0.10	0
$\tau_{Z_{end}}$	1.94 ± 0.12	2.2	0.04 ± 0.06	0
$\tau_{R_{G\parallel}}$	1.94 ± 0.07	2.2	2.20 ± 0.15	2.5

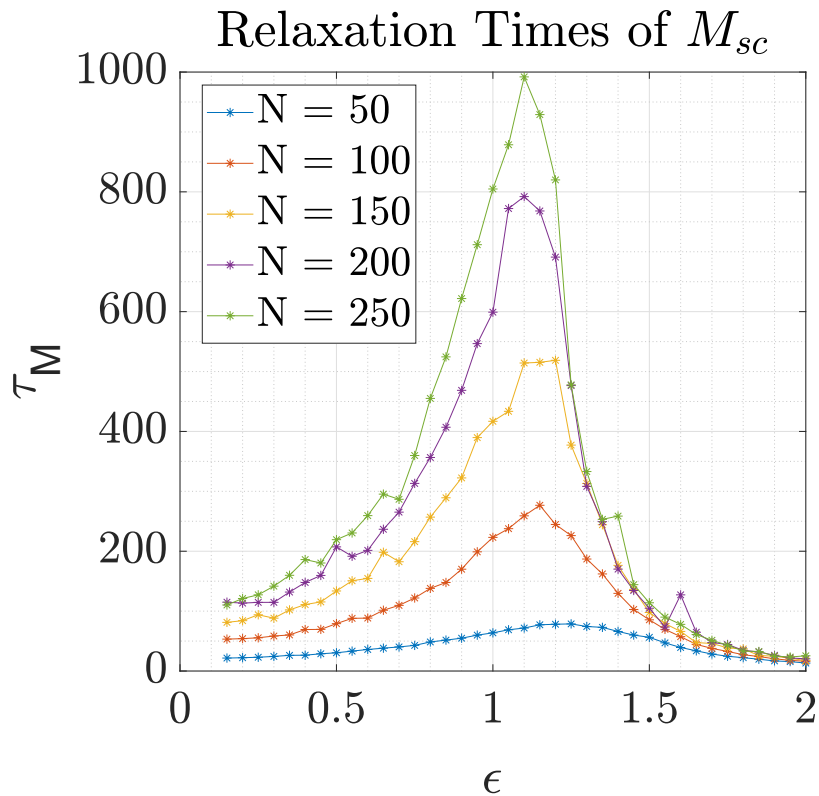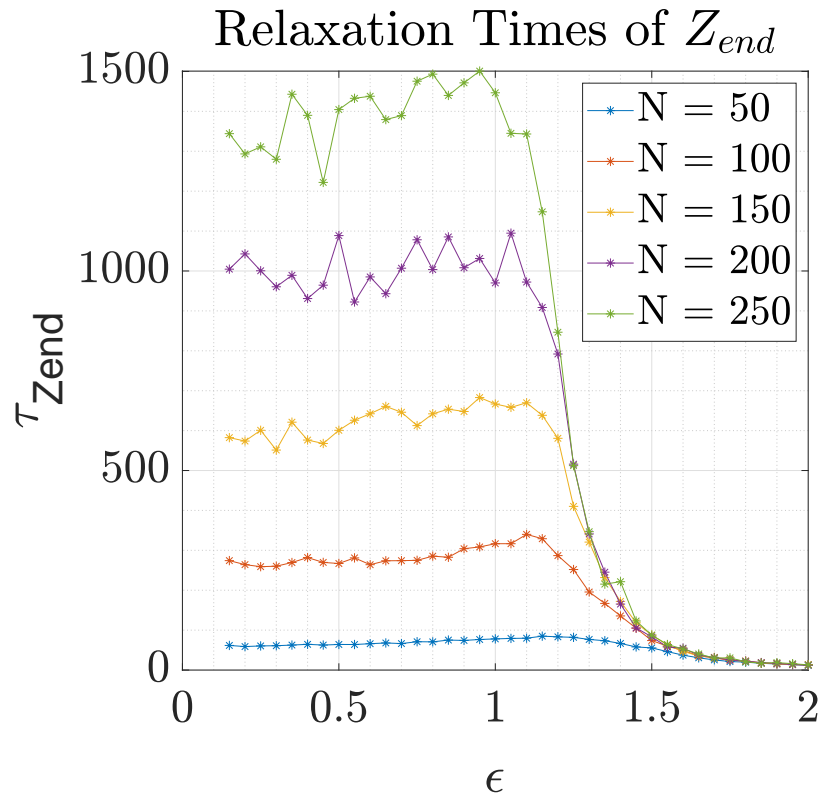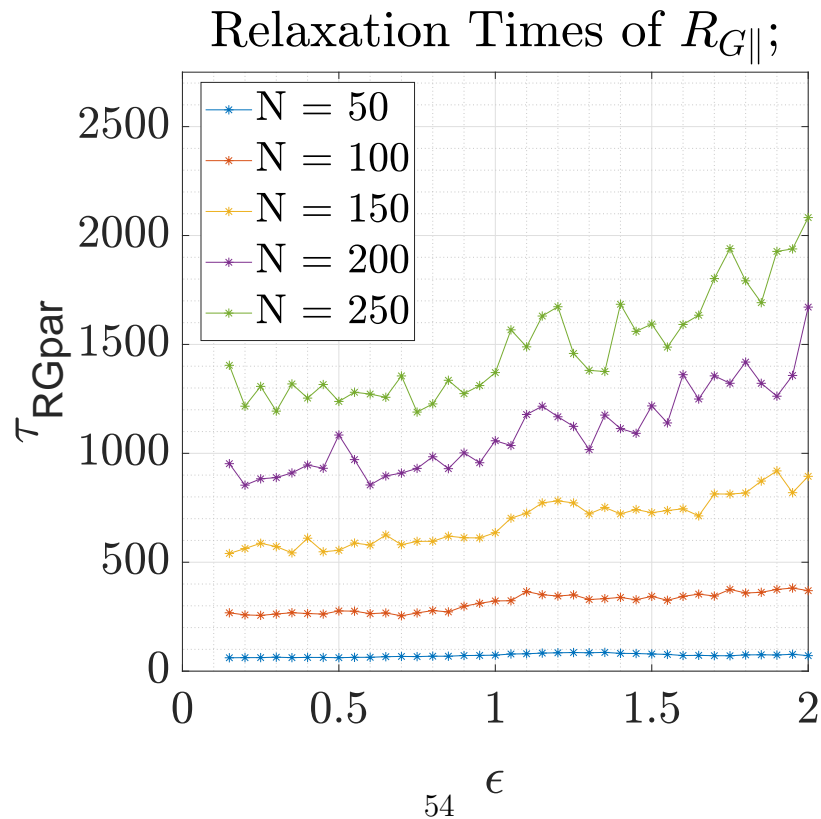Table 4.6: Scaling exponents for the N-dependence of the relaxation times τ_M, $\tau_{Z_{end}}$, and $\tau_{R_{G\parallel}}$, in the vicinity of the transition point, along with the theoretical predictions. $N = 50, 100, 150, 200, 250$.

	Critical Point Region			
	$\epsilon = 1.00$	$\epsilon = 1.05$	$\epsilon = 1.10$	Theoretical Prediction
τ_{Msc}	1.58 ± 0.11	1.63 ± 0.13	1.66 ± 0.12	$1 + 2\phi \approx$ 1.966
$\tau_{Z_{end}}$	1.81 ± 0.11	1.80 ± 0.14	1.70 ± 0.15	2.2
$\tau_{R_{G\parallel}}$	1.84 ± 0.14	1.85 ± 0.10	1.80 ± 0.15	2.2

The scaling for the relaxation times with N does not agree as neatly with the theoretical predictions as in the previous parts. While τ_{Msc} in the desorption regime and $\tau_{Z_{end}}$ and $\tau_{R_{G\parallel}}$ in the adsorption regime all agree with the expectations, all the other values in all three regimes were underestimated by our simulations or analysis (or both). This error can be caused by a number of reasons. The first is the limited sampling that we are able to achieve. Running the simulations for much longer times can increase the accuracy of our results, however we did not have the time needed for such simulation runs in the present work. A second

possible reason for this skew is the method used to obtain the relaxation times. The best way in principle to get the slowest times of relaxation is to plot the logarithms of the auto-correlation functions against linear time, find the most linear parts with the smallest apparent slopes, and get those slopes by fitting to a straight line. Two reasons pushed us to use a different method, one where we simply integrate the correlation functions giving us an estimate of the mean time of relaxation, which is a mean of the relaxation times of all different processes happening in the system. Since we are interested in the slowest time, and since said mean's main contribution comes from said slowest times, we can use the integration instead. The two reasons we did not go by fitting the logarithm of each correlation function are: firstly, we did attempt it for τ_M earlier during this work, and found that it was not as reliable as we expected. An example can be seen in figure 4.18. The times calculated from integration are systematically all less than those obtained from the slopes method. This is to be expected since the integration gives an averaged time instead of the slowest one. However, as is evident in figure 4.18, the slopes method is prone to a high degree of uncertainty due to it largely depending on estimation. The second reason we went with the integration method is the sheer number of correlation functions we would need to manually fit to get the slopes, since the linear parts do not all fall in the same regions. This means that the process cannot be automated, and for every correlation function —as in for every energy, for every N, for every quantity— we need to do the fit independently. This was not doable in the time-frame of the present thesis.
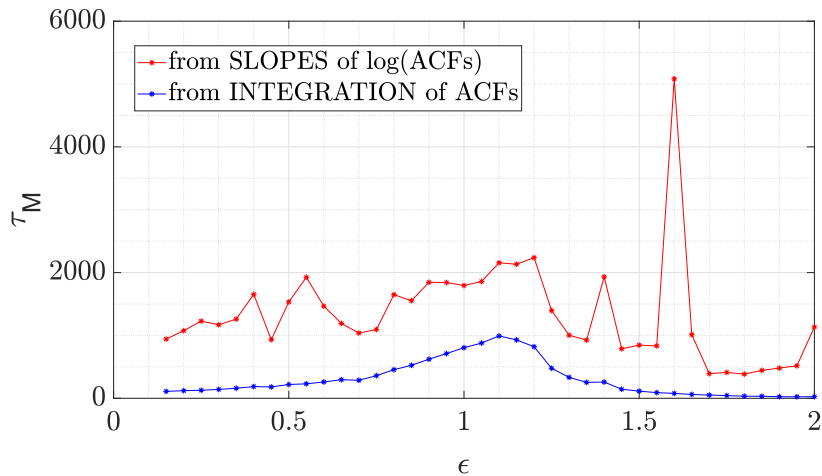
Figure 4.18: Relaxation times of M as found from two different methods; the blue line shows the values achieved from integrating the correlation functions, while the red line shows the values gotten from a visual search of the most linear part of the logarithm of the correlation functions, with the smallest slope.

4.4 A Look at Local Behaviors of the System

Up until now we have been only looking at the system from a global perspective, where all the parameters monitored were defined in the global sense of the whole chain. In this section, we will look at two new quantities, the correlation time of adsorption of any (or of the mean) monomer τ_i, and the correlation distance-along-the-chain of adsorption ξ. We will also investigate the validity of the blob picture in the strong adsorption regime.

4.4.1 Adsorption Correlation Times and Distances for Individual Monomers

We begin by showing a sample of the correlation functions of the adsorption of individual monomers against time (4.19), and of the correlation functions of adsorption of individual monomers *along the chain*, as in against the monomer

index i (4.20).

Time-CF of Adsorption of single monomer for N =250(simple counting)
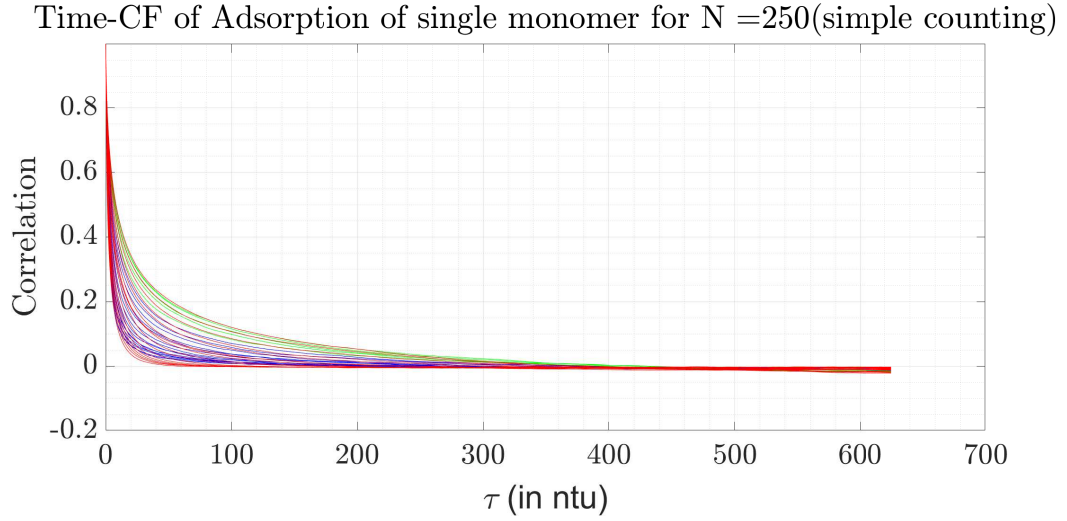
Figure 4.19: Time correlation functions of individual monomers' adsorption events for a chain of 250 monomers, shown for all values of ϵ. Same color scheme as figure 4.12.

CF of Adsorption along the chain for N =150(simple counting)
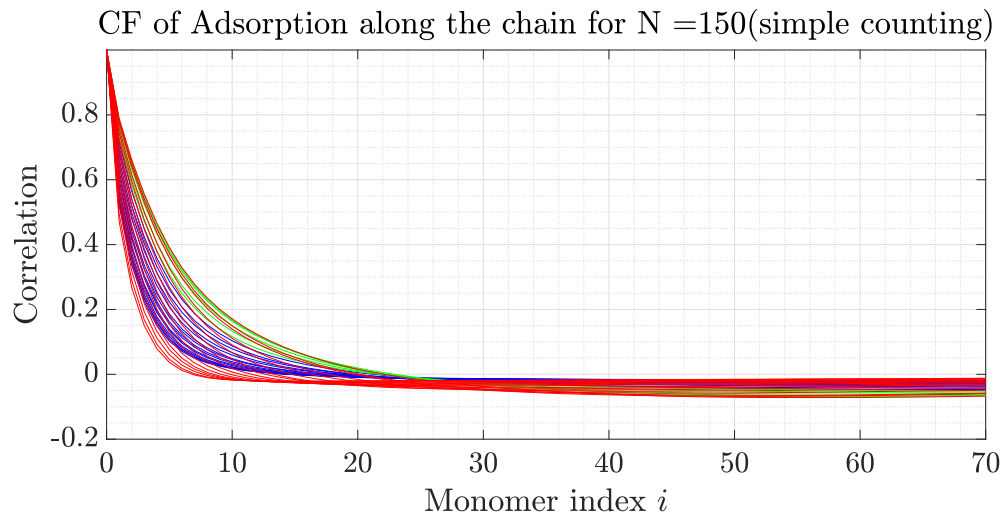
Figure 4.20: Correlation functions of individual monomers' adsorption events along the chain (against distance along the chain) for a chain of 150 monomers, shown for all values of ϵ. Same color scheme as figure 4.12.

It can be noted from both that correlations decay slower the closer we are to the critical point. For a more quantitative evaluation, we plot the found

times and lengths of said correlations in figures 4.21 and 4.22, achieved in by the same integration method. We remind that correlation lengths are obtained from correlation functions that have no time lag; we are calculating the correlation between different monomers at the same instant in time.
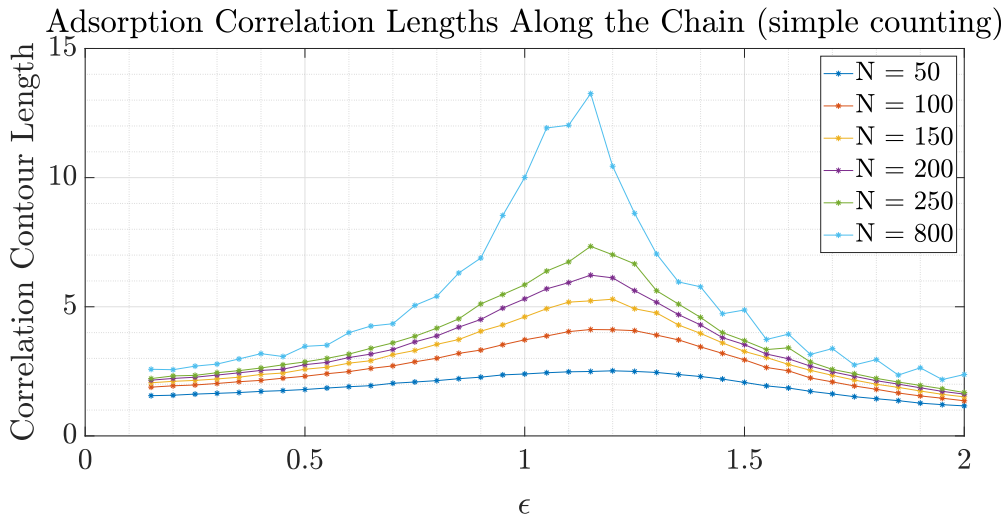
Figure 4.21: Correlations between different monomers' individual adsorption events in units of distance along the chain, for different values of N.

Figure 4.22: Correlation times between different monomers' individual adsorption events, for different values of N.

Theoretical predictions tell us that fluctuations and correlation lengths be-

come of the size of the whole chain at the critical point. This is severely under-realized in our work, where we see that correlations along the chain peak at a value of nearly 14 monomers, for a chain of 800 monomers near the critical point (figure 4.21). For further i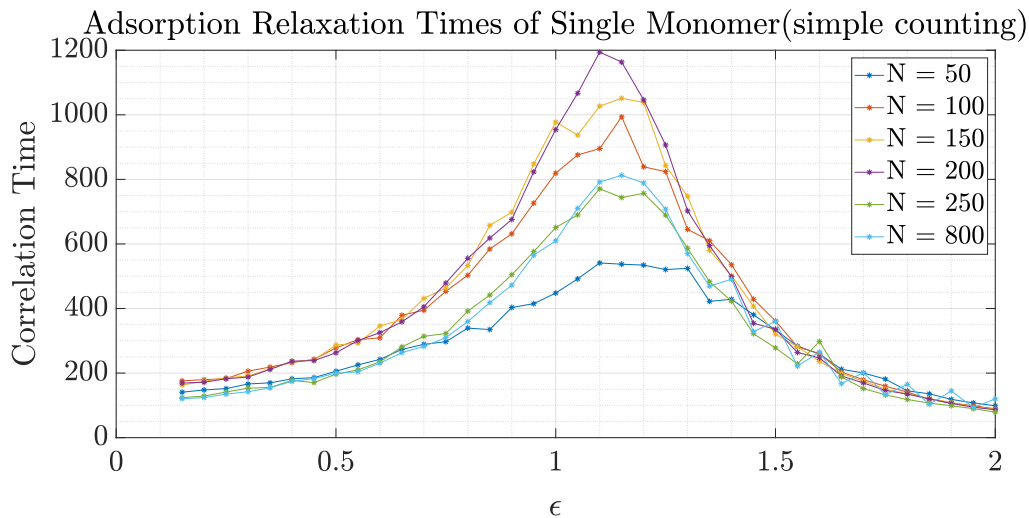nvestigation, we compare our correlation functions of ϵ in the critical vicinity to a theoretical estimate 2.4, both for $N = 800$ (figure 4.23). What we see is a good fit for small along-the-chain distances, which becomes worse progressively with increasing backbone distance. Our simulation correlations reach zero faster than the theoretical prediction. A possible reason for this is the discreteness of our energy axis. Since we only look at quantities for ϵ multiples of 0.05, it is very likely that our functions need corrections because of our distance from the actual critical point. A quick calculation tells us that our rescaled maximum distance from the critical point can be $\frac{0.05/2}{1.11} * N^\phi = 1.24$, if we use $\phi = 0.6$. This rescaled maximum distance is actually quite significant when we look at figure 4.10. This means that the resolution of the energy in our simulations is low, and that we can expect that even our nearest correlation functions to the critical energy will not give a great fit to the theory. However, we can also see that our simulation results are well behaved up to some corrections to scaling.

As for the relaxation times, one issue to be noted is how the curves are not monotone in N; the adsorption relaxation time for a single monomer as a function of ϵ is systematically larger for $N = 100, 150, 200$ than for $N = 250, 800$. In order to see any trend in these plots easily, we can plot the ratio τ_{mi}/τ_M, as seen in figure 4.24. Despite the noise, it is evident that the ratios for different chain lengths converge to a certain small range (between 0.1 and 0.35) in the adsorption regime. It is not exactly clear if the ratios for different N are converging to the same value, however, due to the fluctuations. Longer simulations and further

averaging could help in determining the limit of this convergence.
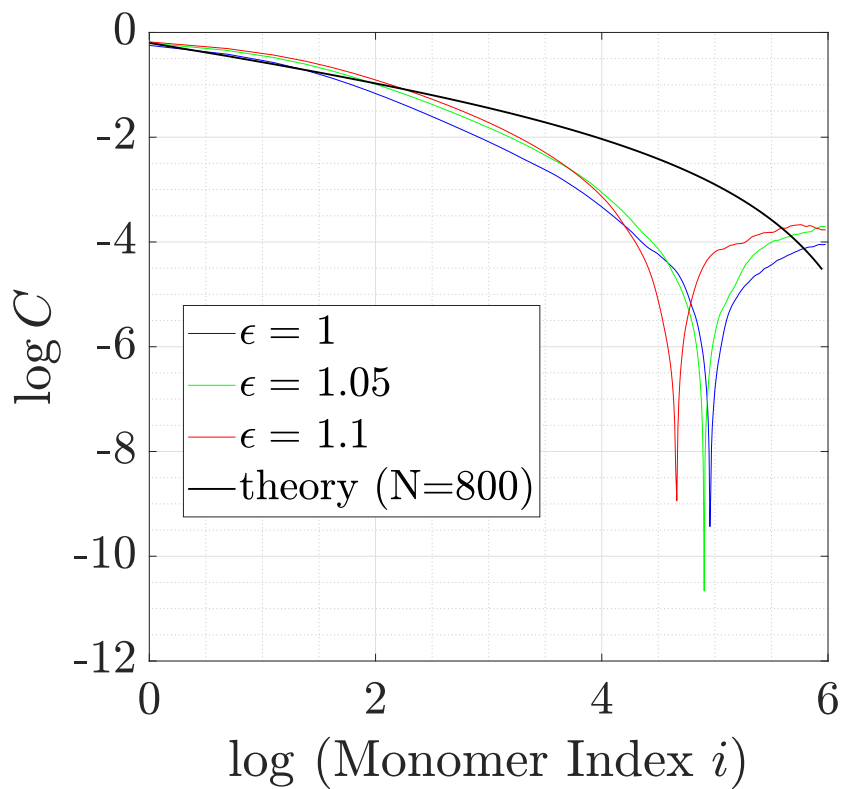
Figure 4.23: Natural logarithm of the along-the-chain correlation functions of individual adsorption events, theoretically at the critical energy (black line), and from simulations at the candidate energies(colored lines).

61
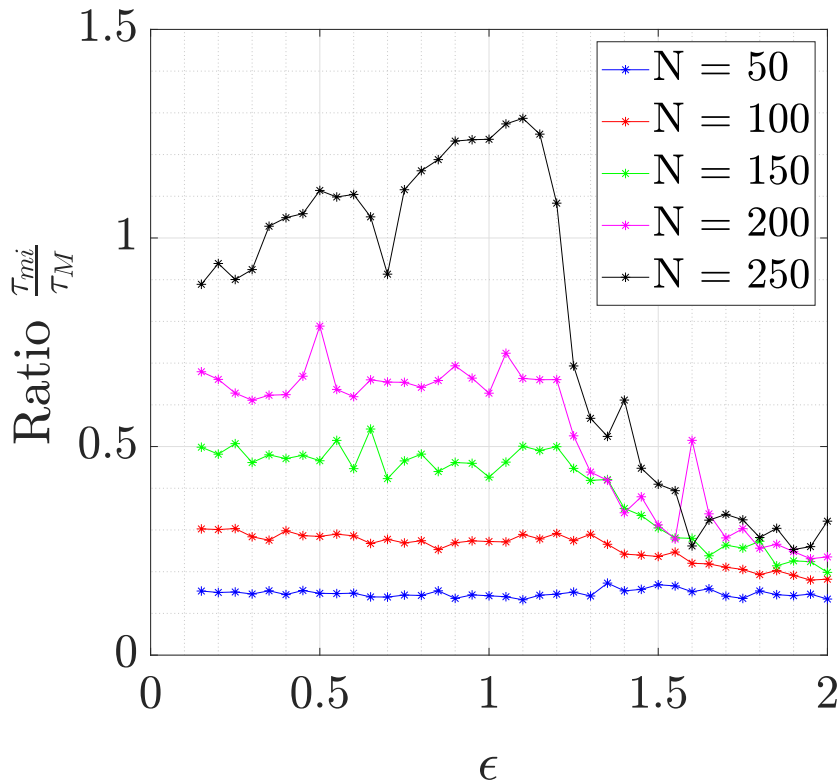
Figure 4.24: Ratio $\frac{\tau_{mi}}{\tau_M}$ as a function of ϵ, for different values of N.

4.4.2 Strong Adsorption Regime and the Blob Picture

To investigate the validity of the hypothesis expanded on in section 2.4, that which expects that the behavior in the adsorption regime obeys the scaling of adsorption blobs, we analyze the dependencies of particularly picked pairs of quantities for $1.5 \leq \epsilon \leq 2.0$.

In figure 4.25 we log-log plot the **along-the-chain** correlation lengths against the mean height of the free end. If the blob picture is to hold, we can expect that

$$\langle Z_{end} \rangle \sim \xi_M \propto g_M^{\nu_{3D}}.$$

This means that a logarithmic plot should give a slope of $1/\nu_{3D} = 1.67$. Looking at said figure, we find that for lower energies (while remaining in the adsorption regime) our data does not fit well the expectation. Surprisingly however, the fit becomes noticeably better for higher energies. This is surprising because the blob idea supposedly works better for weak adsorption and (relatively) large blobs (as in blobs of many monomers as opposed to one or two). Here, our "blob" fit is describing smaller blobs better than larger ones.
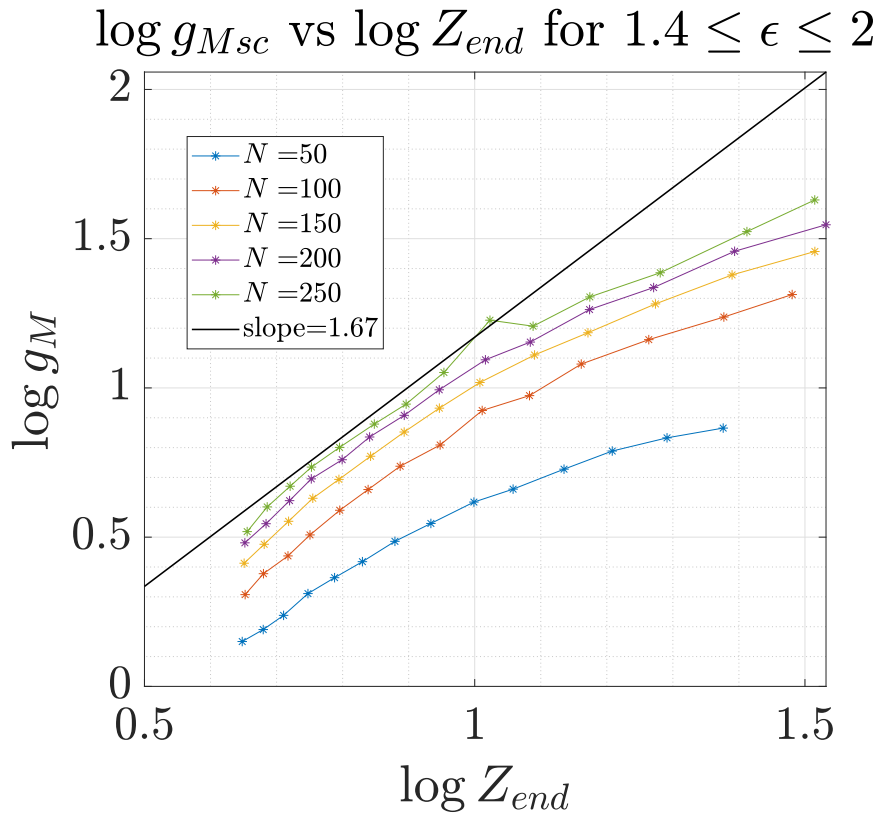
Figure 4.25: log-log graph of the correlation length (of adsorption events) along the chain g_M against Z_{end} in the adsorption regime, with theoretical slope shown by the black line.

Next we look at how relaxation times are related in the adsorption regime. We plot $\tau_{Z_{end}}$ against τ_{Msc} in figure 4.26. The lines for different N's seem to be

in relatively good agreement with the expectation of $slope = 1$.
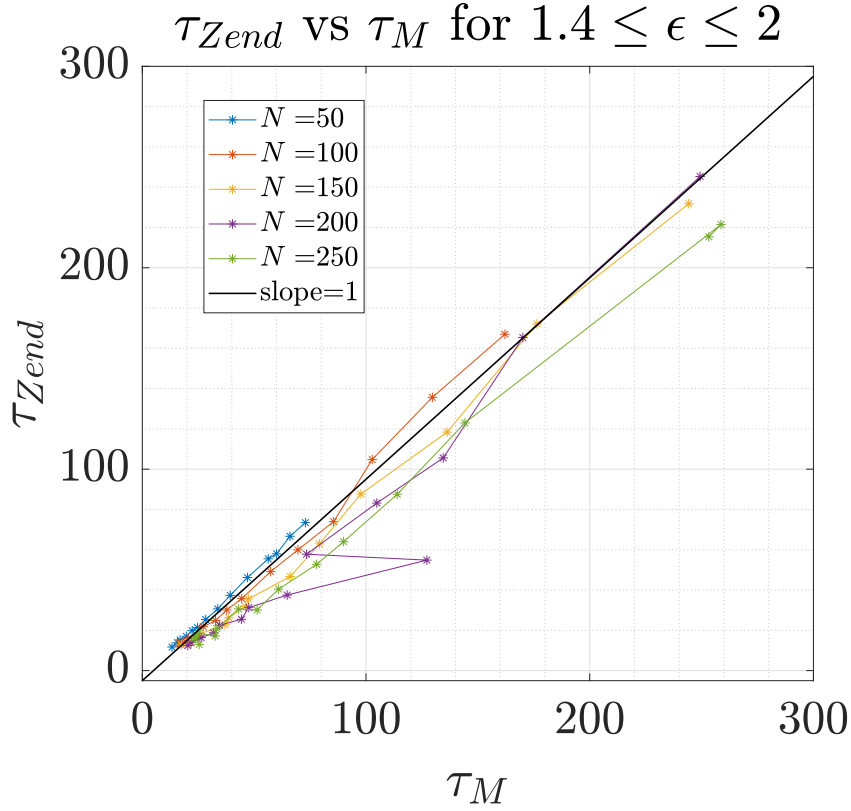
Figure 4.26: Relaxation time of Z_{end} against that of M in the adsorption regime $(1.4 \leq \epsilon \leq 2)$, with theoretical slope shown by the black line.

Furthermore, if the system is in fact governed by blob scaling in the adsorption regime, it can be shown in fact that(as we do in 2.4)

$$\tau_{Z_{end}} \propto \langle Z_{end} \rangle^{2+\frac{1}{\nu_{3D}}} \approx \langle Z_{end} \rangle^{3.67},$$

and that

$$\tau_{R_{G\parallel}} \propto \langle Z_{end} \rangle^{2-2\frac{\nu_{2D}}{\nu_{3D}}} \approx \langle Z_{end} \rangle^{-0.5}.$$

Figures 4.27 and 4.28 expose those very dependencies, giving visually pleasing

fits as can be seen.

For the more useful quantitative analysis we turn the reader's attention to table 4.7, which presents all the relevant scaling laws and dependencies along with uncertainties and theoretical predictions.

Figure 4.27: Relaxation time of Z_{end} against Z_{end} in the adsorption regime, with theoretical slope shown by the black line.

Our simulations return values that are systematically smaller than the expected 1.67 for the slope of $\log g_{Msc}$ against $\log Z_{end}$, for the values of N considered here; only for $N = 250$ does the expectation fall within the uncertainty range obtained. However, with few exceptions, the slopes calculated for the rest of the variables are well within reasonable range to the theoretical predictions.
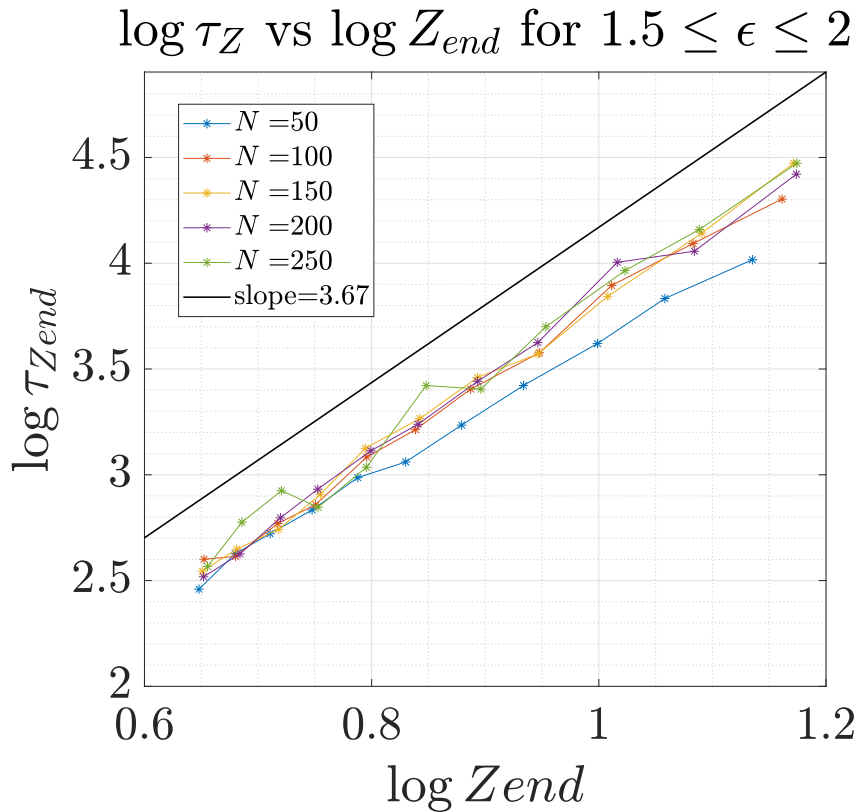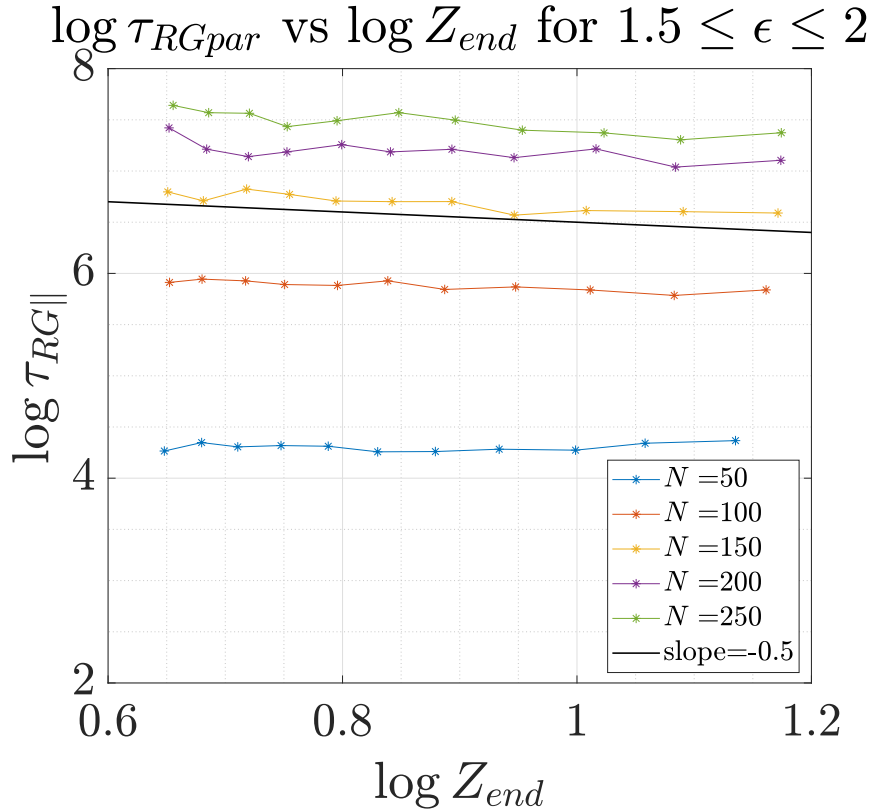
Figure 4.28: Relaxation time of $R_{G\parallel}$ against Z_{end} in the adsorption regime, with theoretical slope shown by the black line.

Our simulations show that in fact τ_{Zend} scales nearly linearly with τ_{Msc}, with that linearity decreasing with increasing N. As for τ_{Zend} and $\tau_{R_{G\parallel}}$ against Z_{end}, we get a clear disagreement for $N = 50$, but very good agreements for all other chain lengths.

The results we have achieved, while mixed, tell us that the validity of the blob picture's description of polymer dynamics is not out of the question, when in the adsorption regime. We have shown that Molecular Dynamics simulation results support to a good extent this description. However, further investigation is necessary, with more care taken to eliminate possible sources of error, such as an alternate method of calculation for the relaxation times, corrections of higher order to scaling, and greater simulation time and averaging.

Table 4.7: Slopes of linear fits of pairs of quantities for different N values, along with the corresponding theoretical predictions.

	$\log g_{Msc}$ vs $\log Z_{end}$ (expected slope = 1.67)	$\tau_{Z_{end}}$ vs τ_M (expected slope = 1)	$\log \tau_{Z_{end}}$ vs $\log Z_{end}$ (expected slope ≈ 3.67)	$\log \tau_{R_{G\parallel}}$ vs $\log Z_{end}$ (expected slope ≈ −0.5)
$N = 50$	1.00 ± 0.20	1.00 ± 0.05	3.16 ± 0.06	0.10 ± 0.20
$N = 100$	1.20 ± 0.20	1.07 ± 0.04	3.54 ± 0.09	-0.24 ± 0.14
$N = 150$	1.20 ± 0.20	0.99 ± 0.13	3.68 ± 0.08	-0.40 ± 0.25
$N = 200$	1.20 ± 0.20	0.97 ± 0.10	3.67 ± 0.12	-0.4 ± 0.4
$N = 250$	1.20 ± 0.25	0.88 ± 0.10	3.62 ± 0.16	-0.5 ± 0.3

4.5 Energy Counting of Adsorption Events

We finally investigate the second method of defining and counting adsorption events. While we previously counted the number of monomers with z-components between 0 and 2.5σ, one can conversely calculate the energetic interaction between all monomers and the surface, and divide that by ϵ. We show in this section the same graphs as for the simple counting but while applying this new definition. Starting with the cumulants in figure 4.29, we calculate the intersection to be at $\epsilon_{ec}^* = 1.012 \pm 0.013$. The two methods give slightly different results, while staying in the general vicinity of $\epsilon = 1$. As for the number of contacts, we show figure 4.30. One important artifact of this counting is the curvature we see at very low energies. This curvature does not express actual increase in the contact number, but is there due to the division by ϵ. This means that energy counting is not reliable in the weak adsorption regime. We can also plot the adsorbed fractions for both counting methods (figure 4.31), which suggests that energy counting

underestimates the number of contacts.
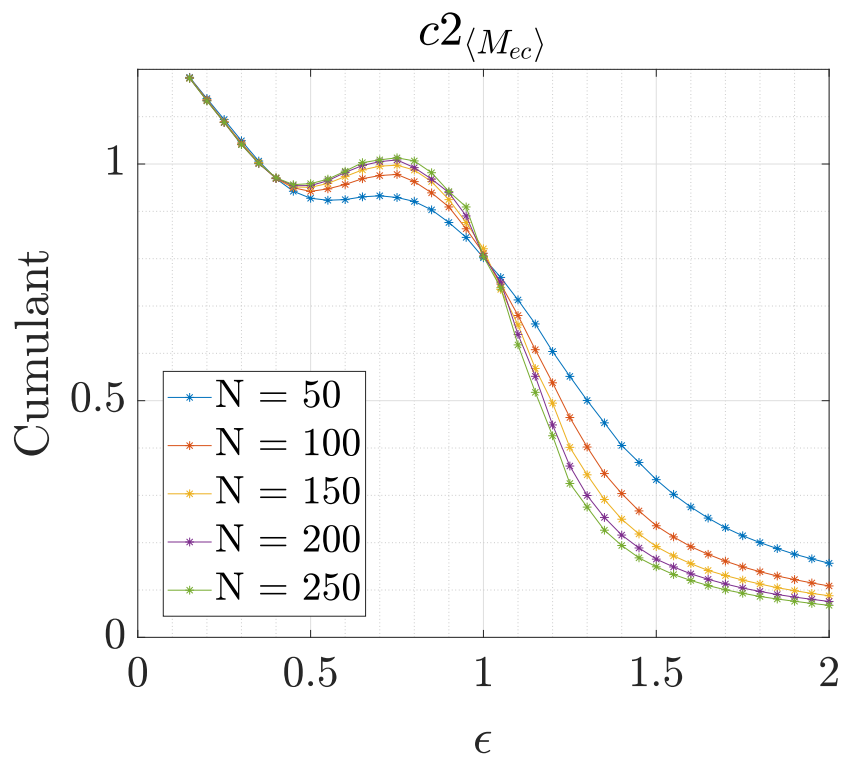
Figure 4.29: Second-order cumulants of adsorption number M_{ec} as counted by energy counting.
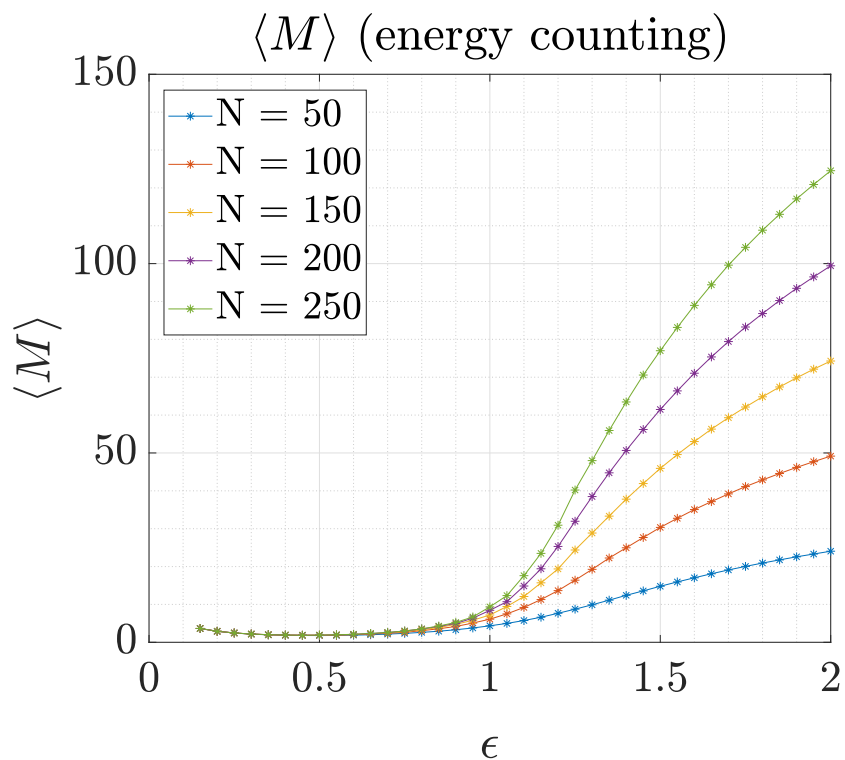
Figure 4.30: Mean number of contacts $\langle M_{ec} \rangle$ as counted by energy counting.
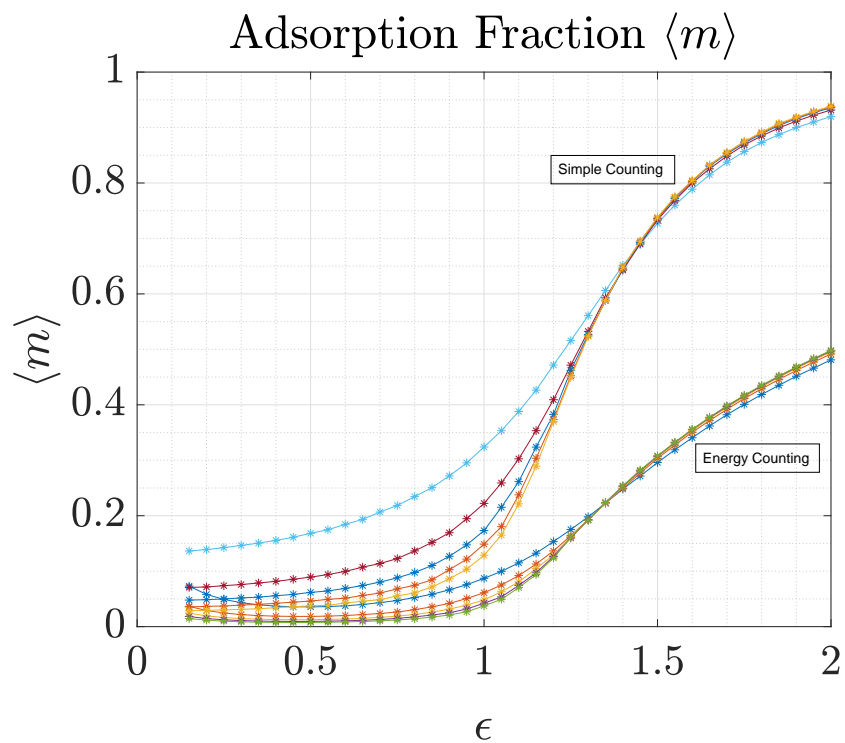
Figure 4.31: Adsorption fraction $\langle m \rangle = \langle M \rangle / N$ for both simple and energy counting methods, as labeled, for $N = 50, 100, 150, 200, 250$.
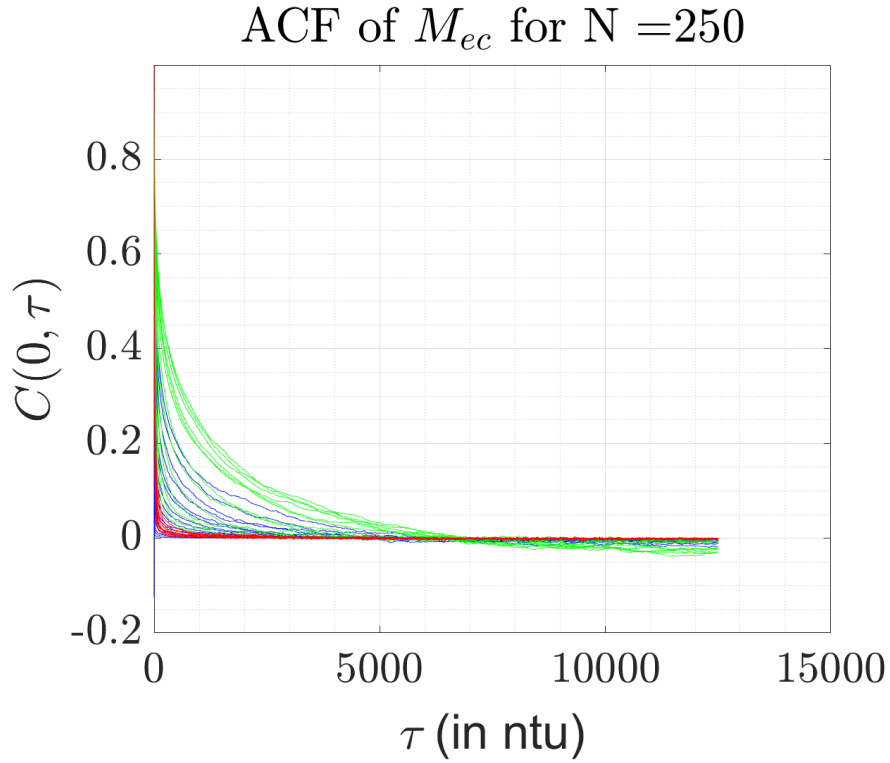
Figure 4.32: Time autocorrelation functions of adsorption number $\langle M_{ec} \rangle$ as counted by energy counting, for all values of ϵ. Same color scheme as figure 4.12.

Lastly, we show a sample of the adsorption correlation functions (figure 4.32), where energy counting was employed to get the number of contacts. Integrating as previously done yields the relaxation times of figure 4.33. We summarize the scaling with N of the three quantities of interest obtained by energy counting in tables 4.8 and 4.9.
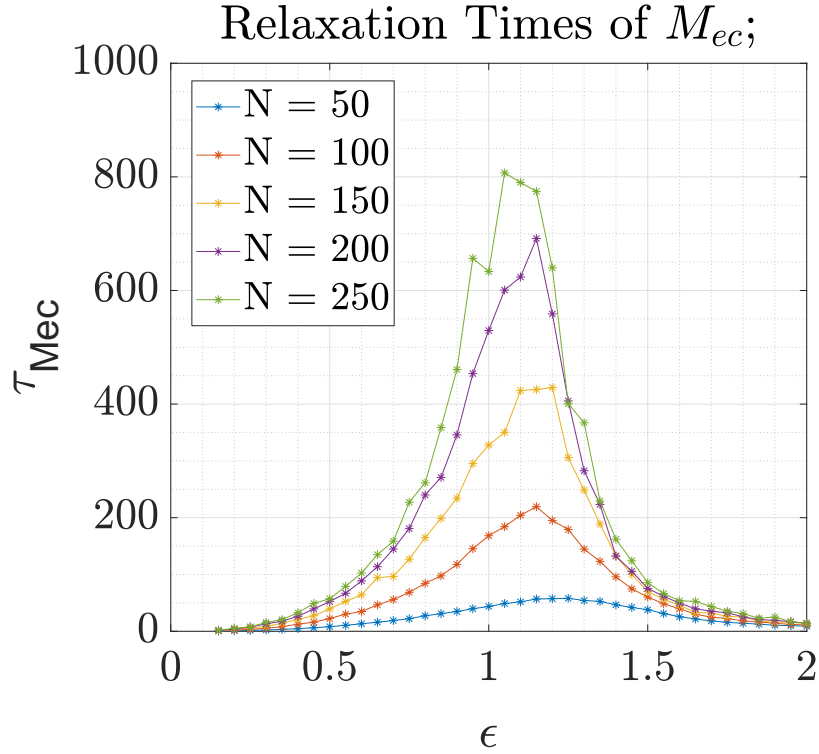
Figure 4.33: Relaxation times gotten by integrating the correlation functions of $\langle M_{ec} \rangle$, as functions of N.

Table 4.8: Scaling exponents for the N-dependence of quantities of interest $\langle M \rangle$, $\langle Z_{end} \rangle$, and $\langle R_{G\|} \rangle$ below and above the transition point, along with the theoretical predictions. $N = 50, 100, 150, 200, 250$.

	Desorption Regime		Adsorption Regime	
	$\epsilon = 0.15$	Theoretical Prediction	$\epsilon = 2.00$	Theoretical Prediction
$\langle M \rangle_{ec}$	$-0.00040 \pm$ 0.00020	0	1.022 ± 0.004	1
σ_{Mec}	-0.0027 ± 0.0007	0	1.000 ± 0.003	0.5
τ_{Mec}	0.84 ± 0.10	1	0.32 ± 0.06	0

Energy counting also gives mixed results. Most estimates of ϕ are bad when looking at either $\langle M \rangle_{ec}$ or σ_{Mec}; however the scaling of τ_{Mec} with N appears to

Table 4.9: Scaling exponents for the N-dependence of quantities of interest $\langle M \rangle$, $\langle Z_{end} \rangle$, and $\langle R_{G\parallel} \rangle$, in the vicinity of the transition point, along with the theoretical predictions. $N = 50, 100, 150, 200, 250$.

	Critical Point Region			
	$\epsilon = 1.00$	$\epsilon = 1.05$	$\epsilon = 1.10$	Theoretical Prediction
$\langle M \rangle_{ec}$	0.473 ± 0.014	0.560 ± 0.020	0.691 ± 0.012	$\phi \approx 0.483$
σ_{Mec}	0.950 ± 0.020	1.090 ± 0.015	1.212 ± 0.004	$\phi \approx 0.483$
τ_{Mec}	1.70 ± 0.14	1.75 ± 0.08	1.72 ± 0.16	$1 + 2\phi \approx 1.966$

be somewhat better. We conclude that energy counting as used in the present work is less reliable than simple counting. It gives partial agreement with the theory when it comes to scaling with N, but poor mean adsorption number in the weak regime. It also underrates the number of contacts in the strong regime, when compared to the more widely used simple counting.

Chapter 5

Conclusion and Future Work

In this work, we ran molecular dynamics simulations to simulate a real chain near an attractive solid interface at equilibrium. While the chain goes through a phase transition as the attraction strength ϵ is varied, we focus our investigation into the adsorption regime, where $\epsilon > \epsilon^*$ and the chain is more likely to be found near the surface. We aimed to check the validity of the adsorption blob argument set out originally by de Gennes [25], by deriving from it scaling laws of system properties. We also attempt to characterize the system in terms of local variables, namely individual monomers' adsorption events.

After ensuring our simulations' consistency with previous known results, pertaining to mean number of adsorbed monomers $\langle M \rangle$, mean height of the chain's free end $\langle Z_{end} \rangle$, and mean parallel-to-surface component of the chain's gyration radius $\langle R_{G\parallel} \rangle$, we investigate the adsorption regime for spatial and temporal dependencies that may strengthen the "blob" argument. Scaling arguments are employed conjointly with the Rouse model to write the expected scaling of correlation lengths and times with measured quantities (see table 2.1).

Very good agreement between our simulations and the adsorption blob theory's predictions is found for $\tau_{Zend} \propto \langle Z_{end} \rangle^{3.67}$, $\tau_{RG\parallel} \propto \langle Z_{end} \rangle^{-0.5}$, and $\tau_{Zend} \propto \tau_M$. The prediction that $\xi_M \sim g_M^{0.67} \propto Z_{end}$ was not properly verified; the power of 0.67 was overestimated for chains of lengths between 50 and 250. In addition, the ratio of the adsorption relaxation time of individual monomers to the relaxation time of M, τ_{mi}/τ_M, was also probed, finding that for different chain lengths the ratios converged in the adsorption regime to a narrow range between 0.1 and 0.35. Lastly, along-the-chain correlation functions were calculated from simulations, giving a profile for correlations' decay along the polymer, as function of the adsorption strength. They were also compared to theoretically derived correlations, where proximity and similarity were evident for short backbone distances.

Future work will investigate the source of the departures from expectations and theory found. An increase in the resolution of the ϵ axis, along with extended simulation time and better averaging are expected to enhance most found scaling laws, both reproducing known results better, and finding local variables more accurately. A better method will also be employed to extract relaxation times from correlation functions. Lastly, the range of validity of the blob argument is worth probing in the adsorption regime.

Bibliography

[1] S. Zhang, S. Qi, L. I. Klushin, A. M. Skvortsov, D. Yan, and F. Schmid, "Phase transitions in single macromolecules: Loop-stretch transition versus loop adsorption transition in end-grafted polymer chains," *The Journal of chemical physics*, vol. 148, no. 4, p. 044903, 2018.

[2] A. M. Skvortsov, A. A. Gorbunov, and L. I. Klushin, "Adsorption-stretching analogy for a polymer chain on a plane. symmetry property of the phase diagram," *The Journal of chemical physics*, vol. 100, no. 3, pp. 2325–2334, 1994.

[3] R. Descas, J.-U. Sommer, and A. Blumen, "Dynamical scaling of single chains on adsorbing substrates: diffusion processes," *The Journal of chemical physics*, vol. 122, no. 13, p. 134903, 2005.

[4] T. Hunt and B. Todd, "A comparison of model linear chain molecules with constrained and flexible bond lengths under planar couette and extensional flows," *Molecular Simulation*, vol. 35, pp. 1153–1167, 12 2009.

[5] "Wikimedia commons, english: 12-6-lennard-jones-potential.svg, retrieved from https://commons.wikimedia.org/wiki/file:12-6-lennard-jones-potential.svg," 2007.

[6] D. Frenkel and B. Smit, *Understanding molecular simulation: from algorithms to applications*, vol. 1. Elsevier, 2001.

[7] G. Binnig, C. F. Quate, and C. Gerber, "Atomic force microscope," *Phys. Rev. Lett.*, vol. 56, pp. 930–933, Mar 1986.

[8] H. J. Kreuzer and M. Grunze, "Stretching of single polymer strands: A first-principles theory," *Europhysics Letters (EPL)*, vol. 55, pp. 640–646, sep 2001.

[9] T. Hugel, M. Rief, M. Seitz, H. E. Gaub, and R. R. Netz, "Highly stretched single polymers: Atomic-force-microscope experiments versus ab-initio theory," *Phys. Rev. Lett.*, vol. 94, p. 048301, Jan 2005.

[10] E.-L. Florin, V. T. Moy, and H. E. Gaub, "Adhesion forces between individual ligand-receptor pairs," *Science*, vol. 264, no. 5157, pp. 415–417, 1994.

[11] A. Serr and R. R. Netz, "Pulling adsorbed polymers from surfaces with the AFM: stickvs.slip, peelingvs.gliding," *Europhysics Letters (EPL)*, vol. 73, pp. 292–298, jan 2006.

[12] F. Oesterhelt, D. Oesterhelt, M. Pfeiffer, A. Engel, H. Gaub, and D. Müller, "Unfolding pathways of individual bacteriorhodopsins," *Science*, vol. 288, no. 5463, pp. 143–146, 2000.

[13] M. Kessler, K. E. Gottschalk, H. Janovjak, D. J. Muller, and H. E. Gaub, "Bacteriorhodopsin folds into the membrane against an external force," *Journal of molecular biology*, vol. 357, no. 2, pp. 644–654, 2006.

[14] F. Kühner, M. Erdmann, and H. E. Gaub, "Scaling exponent and kuhn length of pinned polymers by single molecule force spectroscopy," *Phys. Rev. Lett.*, vol. 97, p. 218301, Nov 2006.

[15] R. A. L. Jones, "Soft condensed matter," *European Journal of Physics*, vol. 23, pp. 652–652, oct 2002.

[16] R. R. Netz and D. Andelman, "Neutral and charged polymers at interfaces," *Physics Reports*, vol. 380, no. 1, pp. 1 – 95, 2003.

[17] E. Eisenriegler, *Polymers near surfaces: conformation properties and relation to critical phenomena.* World Scientific, 1993.

[18] G. Fleer, J. Scheujtens, M. ohen Stuart, B. Vincent, and T. Cosgrove, "Polymers at interfaces, chapman hall," *London-Glasgow-New York*, 1993.

[19] H. Frisch, R. Simha, and F. Eirich, "Statistical mechanics of polymer adsorption," *The Journal of Chemical Physics*, vol. 21, no. 2, pp. 365–366, 1953.

[20] R. J. Rubin, "Randomwalk model of chainpolymer adsorption at a surface," *The Journal of Chemical Physics*, vol. 43, no. 7, pp. 2392–2407, 1965.

[21] Y. Lépine and A. Caillé, "The configuration of a polymer chain interacting with a plane interface," *Canadian Journal of Physics*, vol. 56, no. 4, pp. 403–408, 1978.

[22] R. Descas, J.-U. Sommer, and A. Blumen, "Static and dynamic properties of tethered chains at adsorbing surfaces: A monte carlo study," *The Journal of chemical physics*, vol. 120, no. 18, pp. 8831–8840, 2004.

[23] A. M. Skvortsov, L. I. Klushin, A. A. Polotsky, and K. Binder, "Mechanical desorption of a single chain: Unusual aspects of phase coexistence at a first-order transition," *Physical Review E*, vol. 85, no. 3, p. 031803, 2012.

[24] M. Rubinstein and R. H. Colby, *Polymer physics*, vol. 23. Oxford university press New York, 2003.

[25] P.-G. De Gennes, *Scaling concepts in polymer physics.* Cornell university press, 1979.

[26] C. Gardiner, *Stochastic methods*, vol. 4. springer Berlin, 2009.

[27] P. Grassberger, "Simulations of grafted polymers in a good solvent," *Journal of Physics A: Mathematical and General*, vol. 38, no. 2, p. 323, 2004.

[28] L. I. Klushin, A. A. Polotsky, H.-P. Hsu, D. A. Markelov, K. Binder, and A. M. Skvortsov, "Adsorption of a single polymer chain on a surface: Effects of the potential range," *Physical Review E*, vol. 87, no. 2, p. 022604, 2013.

[29] L. Klushin and A. Skvortsov, "Unconventional phase transitions in a constrained single polymer chain," *Journal of Physics A: Mathematical and Theoretical*, vol. 44, no. 47, p. 473001, 2011.

[30] S. Metzger, M. Müller, K. Binder, and J. Baschnagel, "Adsorption transition of a polymer chain at a weakly attractive surface: Monte carlo simulation of off-lattice models," *Macromolecular theory and simulations*, vol. 11, no. 9, pp. 985–995, 2002.

[31] E. Eisenriegler, K. Kremer, and K. Binder, "Adsorption of polymer chains at surfaces: Scaling and monte carlo analyses," *The Journal of Chemical Physics*, vol. 77, no. 12, pp. 6296–6320, 1982.

[32] I. Gerroff, A. Milchev, K. Binder, and W. Paul, "A new off-lattice monte carlo model for polymers: A comparison of static and dynamic properties with the bond-fluctuation model and application to random media," *The Journal of chemical physics*, vol. 98, no. 8, pp. 6526–6539, 1993.

[33] A. Milchev, W. Paul, and K. Binder, "Off-lattice monte carlo simulation of dilute and concentrated polymer solutions under theta conditions," *The Journal of chemical physics*, vol. 99, no. 6, pp. 4786–4798, 1993.

[34] N. Korolev, L. Nordenskioeld, and A. P. Lyubartsev, "Multiscale coarse-grained modelling of chromatin components: Dna and the nucleosome," *Advances in colloid and interface science*, vol. 232, pp. 36–48, 2016.

[35] S. Kmiecik, D. Gront, M. Kolinski, L. Wieteska, A. E. Dawid, and A. Kolinski, "Coarse-grained protein models and their applications," *Chemical Reviews*, vol. 116, no. 14, pp. 7898–7936, 2016. PMID: 27333362.

[36] L. Verlet, "Computer" experiments" on classical fluids. i. thermodynamical properties of lennard-jones molecules," *Physical review*, vol. 159, no. 1, p. 98, 1967.